

Testing Anomalous Gauge Couplings of the Higgs Boson via Weak-Boson Scatterings at the LHC

Bin Zhang

Department of Physics, Tsinghua University, Beijing 100084, China.

Yu-Ping Kuang

*China Center of Advanced Science and Technology (World Laboratory), P.O.Box 8730, Beijing 100080, China;
Department of Physics, Tsinghua University, Beijing 100084, China.**

Hong-Jian He

Center for Particle Physics, University of Texas at Austin, Austin, Texas 78712, U.S.A.

C.-P. Yuan

*Department of Physics and Astronomy, Michigan State University, East Lansing, MI 48824, U.S.A.
(TUHEP-TH-01127, UTHEP-03-13, MSUHEP-030103)*

We propose a sensitive way to test the anomalous HVV couplings ($V = W^\pm, Z^0$) of the Higgs boson (H), which can arise from either the dimension-3 effective operator in a nonlinearly realized Higgs sector or the dimension-6 effective operators in a linearly realized Higgs sector, via studying the VV scattering processes at the CERN LHC. The gold-plated pure leptonic decay modes of the final state weak bosons in the processes $pp \rightarrow VVjj$ are studied. For comparison, we also analyze the constraints from the precision electroweak data, the expected precision of the measurements of the Higgs production rate, decay width and branching ratios at the Tevatron Run-2 and the LHC, and the requirement of the unitarity of the S -matrix. We show that, with an integrated luminosity of 300 fb^{-1} and sufficient kinematical cuts for suppressing the backgrounds, studying the process $pp \rightarrow W^+W^+jj \rightarrow \ell^+\nu\ell^+\nu jj$ can probe the anomalous HWW couplings at a few tens of percent level for the nonlinearly realized Higgs sector, and at the level of $0.01 - 0.08 \text{ TeV}^{-1}$ for the linearly realized effective Lagrangian.

PACS number(s): 14.65.Ha, 12.15.Lk, 12.60.Nz

I. INTRODUCTION

The Standard Model (SM) of the electroweak interactions has proved to be very successful in explaining all the available experimental data at the scale $\lesssim \mathcal{O}(100) \text{ GeV}$. However, the mechanism of the electroweak symmetry breaking (EWSB) remains as one of the most profound puzzles in particle physics. The Higgs sector of the SM suffers the well-known problems of triviality [1] and unnaturalness [2], therefore there has to be new physics beyond the SM above certain high energy scale Λ . Within the SM formalism, the precision electroweak data favors a light Higgs boson. If a light Higgs boson candidate H is found in the future collider experiments, such as the Run-2 of the Fermilab Tevatron, a $2 \text{ TeV } p\bar{p}$ collider, or the CERN Large Hadron Collider (LHC), a $14 \text{ TeV } pp$ collider, the next important task is to experimentally measure

the gauge interactions of this Higgs scalar and explore the nature of the EWSB mechanism. The detection of the anomalous gauge couplings of the Higgs boson will point to the new physics beyond the SM underlying the EWSB mechanism.

Although the correct theory of new physics is not yet clear, the effect of any new physics at energy below the cutoff scale Λ can be parametrized as effective interactions in an effective theory whose particle content is the same as the SM. This provides a model-independent description, and the anomalous couplings relative to that of the SM reflect the effect of new physics. In the present study, we assume that all possible new particles other than the lightest Higgs boson H are heavy and around or above the scale Λ , so that only H is relevant to the effective theory. Therefore, testing the effective anomalous gauge couplings of the Higgs boson can discriminate the EWSB sector of the new physics model

from that of the SM. It has been pointed out that sensitive tests of the anomalous HVV couplings (with $V = W^\pm, Z^0$) can be performed via Higgs boson productions at the future high energy e^+e^- linear colliders (LC) [3,4]. The tests of the anomalous HVV couplings at hadron colliders via the decay mode $H \rightarrow \gamma\gamma$ and $H \rightarrow \tau\tau$ have also been studied, and the obtained sensitivities are lower than that at the LC [6–8].

In this paper, following our recent proposal [9], we study an additional way to test the anomalous HVV couplings via the weak-boson scatterings at the LHC. We shall show that at the LHC, rather sensitive tests of the anomalous HVV couplings can be obtained by measuring the cross sections of the longitudinal weak-boson scattering, $V_L V_L \rightarrow V_L V_L$ ($V_L = W_L^\pm, Z_L^0$), especially $W_L^+ W_L^+ \rightarrow W_L^+ W_L^+$. The scattering amplitude contains two parts: (i) the amplitude $T(V, \gamma)$ related only to the electroweak gauge bosons as shown in Fig. 1(a), and (ii) the amplitude $T(H)$ related to the Higgs boson as shown in Fig. 1(b). At high energies, both $T(V, \gamma)$ and $T(H)$ contain a piece increasing with the center-of-mass energy (E) as E^2 in the nonlinear realization and as E^4 in the linear realization. In the SM, though the individual diagram in Fig. 1(a) may contribute a E^4 -dependent piece, the sum of all diagrams in Fig. 1(a) can have at most E^2 -dependent contribution, which can be easily verified by an explicit calculation. Furthermore, the HVV coupling constant in the SM is fixed to be the same as the non-Abelian gauge self-coupling of the weak bosons. This causes the two E^2 -dependent pieces precisely cancel with each other in the sum of $T(V, \gamma)$ and $T(H)$, resulting in the expected E^0 -behavior for the total amplitude, as required by the unitarity of the SM S -matrix. If the HVV couplings are anomalous due to the effect of new physics above the cutoff scale Λ , the total amplitude of VV scatterings can grow as E^2 or E^4 in high energy regime. Such deviations from the E^0 behavior of the SM amplitude can provide rather sensitive test of the anomalous HVV couplings in high energy VV scattering experiments. This type of tests require neither the detection of the Higgs boson resonance nor the measurement of the Higgs boson decay branching ratios, and is thus of special interest. If the anomalous HVV coupling associated with new physics effect is rather large, the total decay width of H may become so large that H cannot be detected as a sharp resonance [10] and therefore escapes the detection when scanning the invariant mass of its decay products around m_H . In that case, can we tell whether there exists a sub-TeV Higgs boson or not? The answer is yes. It can be tested by carefully studying the scatterings of weak gauge bosons in the TeV region [12]. Furthermore, if the new physics causes a rather small HVV coupling

(much below the value of the SM HVV coupling), the production rate of a light Higgs boson can become so small that it escapes the detection when the experimental measurement is taken around the Higgs boson mass scale. However, as mentioned above, the scattering of $V_L V_L$ has to become large in the TeV region accordingly. Therefore, this makes it important to study the $V_L V_L$ scattering in the TeV regime even in the case where a light Higgs boson exists in the EWSB sector. In Sec. IV, we show that this type of test of the anomalous HVV couplings can be more sensitive than those obtained from studying the on-shell Higgs boson production and decays at the LHC [6–8], as well as the constraints derived from the precision electroweak data and the requirement of the unitarity of the S -matrix. Therefore, *studying the $V_L V_L$ scatterings at the LHC is not only important for probing the strongly interacting electroweak symmetry breaking sector without a light Higgs boson, but also valuable for sensitively testing of the anomalous gauge interactions of the Higgs boson when a light Higgs scalar exists in the mass range 115–300 GeV.* This further supports the “no-lose” theorem [11] for the LHC to decisively probe the EWSB mechanism.

This paper is organized as follows. In Sec. II, we briefly sketch a few key points related to the calculations of the VV scatterings discussed in this paper. In Sec. III, we systematically study the test of the anomalous HVV coupling from the dimension-3 operator in a nonlinearly realized Higgs sector [13], as an extension of [9]. The test of the anomalous HVV couplings from the dimension-6 operators in the linearly realized Higgs sector [14,15] is studied in Sec. IV. In both cases, the constraints on the anomalous HVV couplings from the precision electroweak data and the requirement of the unitarity of the S -matrix are also discussed. Sec. V summarize our concluding remarks.

II. VV SCATTERINGS

As mentioned in the previous section, we will take the enhanced VV scatterings as the signals for testing the anomalous HVV couplings. We choose the gold-plated pure leptonic decay modes of the final state weak bosons as the tagging modes, this will avoid the large hadronic backgrounds at the LHC. Even in this case, there are still several kinds of backgrounds to be eliminated, namely the *electroweak (EW) background*, the *QCD background*, and the *top quark background* studied in Refs. [16,17]. At the LHC, the initial state V 's in the VV scattering are emitted by the quarks in the protons. As Refs. [16–19] pointed out, the QCD background can be greatly suppressed by tagging a

forward-going jet (the out-going quark after emitting the V). This forward-jet tagging will also suppress the transverse component (V_T) of the initial V , so that the initial state V will be essentially V_L . Following Refs. [16,17], we impose, in addition to *forward jet tagging*, the requirement of *vetoing the central jet* to further suppress the QCD background and the top quark background. The EW background can be suppressed by *detecting isolated leptons with large transverse momentum in the central rapidity region*, especially requiring the two final state leptons to be nearly back to back. These leptonic cuts also suppress the V_T contributions in the final state. Moreover, choosing the decay leptons in the central rapidity region also avoids the collinear divergence in the diagrams exchanging a photon in $T(V, \gamma)$.

In this paper, we shall calculate the complete tree level contributions to the processes

$$pp \rightarrow VVjj, \quad (1)$$

where j is the forward jet. We shall impose all the cuts mentioned above, and use the updated CTEQ6L [20] parton distribution functions for the distributions of quarks in the protons. We also take into account the effect of the width of the weak boson in calculating the helicity amplitudes.

Ref. [16,17] studied various strongly interacting models which do not consist of a light Higgs boson and the $V_L V_L \rightarrow V_L V_L$ scattering amplitudes are largely enhanced (by powers of E^2) in the high energy region. The signal amplitudes were calculated in the effective W approximation (EWA) [21] because the $V_L V_L \rightarrow V_L V_L$ scattering amplitudes predicted by those models violate the unitarity condition of a $2 \rightarrow 2$ scattering matrix so that a full $2 \rightarrow 4$ process $pp \rightarrow V_L V_L jj$ could not be reliably calculated to predict the signal event rates in the TeV region. Instead, the $V_L V_L \rightarrow V_L V_L$ scattering amplitudes were properly unitarized before they were convoluted with the W -boson luminosities obtained from the EWA to predict the signal event rates. With this method of calculation, it was shown that after imposing the kinematic requirements discussed above, the backgrounds are reasonably suppressed relative to the signals, so that the $V_L V_L$ scatterings signals can be effectively extracted.

As to be discussed in Secs. III and VI, in our present case, the Higgs boson is light, and new physics effect is assumed to only modify the effective operators in either a nonlinearly or a linearly realized Higgs sector. In the nonlinearly realized case, the $V_L V_L$ scattering amplitudes with a not too small anomalous HVV couplings are also enhanced in the high energy region due to the E^2 behavior of the amplitudes. Hence,

we may apply the same methodology as proposed in Ref. [17] for calculating the signal rate. However, in this work, we shall not choose using the EWA. Instead, we shall compute the full $pp \rightarrow VVjj$ cross sections at the tree level, cf. Eq.(1), which is justified as long as the LHC sensitivity to the size of the anomalous HVV coupling is smaller than what required to render the unitarity of the $V_L V_L \rightarrow V_L V_L$ partial wave amplitudes. As to be shown in Secs. IV and VI, this is indeed the case and the backgrounds can be reasonably suppressed relative to the signals by imposing the same kinematical cuts suggested in Ref. [17]. On the contrary, in the case of the SM (without anomalous HVV couplings), all the $V_L V_L$, $V_T V_L$, and $V_T V_T$ amplitudes behave as E^0 rather than E^2 . Because the probability of finding a transverse vector boson with high momentum is much larger than a longitudinal vector boson [21], the contribution of $V_L V_L \rightarrow V_L V_L$ to the production rate of $pp \rightarrow VVjj$ in the TeV region is small as compared to the $V_T V_L$ and $V_T V_T$ contributions. Therefore, although the imposed kinematics cuts can effectively suppress the QCD and the top quark backgrounds, they leave a considerable EW background (mainly originated from the $V_T V_L$ and $V_T V_T$ contributions) that dominates the VV scattering in the SM. Throughout this paper, we will call these VV scattering contributions the remaining SM electroweak backgrounds after imposing the kinematical cuts. We shall do a complete tree-level calculation for both the signal and the background processes with the improvement on the simulation of the kinematical distributions of the decay leptons, and the cross section calculation with the updated parton distribution functions [20] and the inclusion of the vector boson width. Furthermore, we do not apply the EWA [21] in our calculations, hence, our results are not identical to those given in Ref. [17], even for the SM case.

In the case of a linearly realized effective Lagrangian, the physics consideration is quite different. As to be shown in Sec. VI, the $V_L V_L \rightarrow V_L V_L$ scattering amplitudes can have not only the E^2 but also the E^4 contributions depending on the process and operator under consideration. Furthermore, both the $V_T V_T \rightarrow V_L V_L$ and $V_L V_T \rightarrow V_L V_T$ scattering amplitudes can also have the E^2 contributions, which should be undoubtedly counted as part of the *signal* rates because those contributions are absent in the SM. Because the luminosity of V_T is larger than the V_L , the contributions from $V_T V_T$ and $V_T V_L$ scatterings cannot be ignored unless the E^4 contributions dominate the E^2 contributions which occur only when both the energy E and the anomalous couplings become large. It implies that including only the $V_L V_L \rightarrow V_L V_L$ contribution with the EWA, as done in Ref. [17], is not adequate in this case,

and a full $2 \rightarrow 4$ calculation should be used to calculate the signal rates. Although it is possible to apply the EWA to include also the $V_T V_T$ and $V_L V_T$ contributions [22] with jet tagging efficiencies (for V_L and V_T , separately) extracted from the study done in Ref. [17], we choose to perform a full $pp \rightarrow VV jj$ tree-level calculation which is justified as long as the unitarity condition is satisfied. Nevertheless, as to be discussed in the end of Sec. VI, we shall apply the EWA, folded with the $VV \rightarrow VV$ scattering amplitudes, to check the high energy behavior of the full $2 \rightarrow 4$ amplitudes which are also verified to be gauge invariant.

III. TESTING ANOMALOUS HVV COUPLING FROM DIMENSION-3 OPERATOR

A. The Anomalous HVV Coupling from Dimension-3 Operator

It is known that there is no anomalous HVV coupling arising from the dimension-3 and dimension-4 gauge invariant operators in the linearly realized effective Lagrangian [14,15]. Here, we consider the nonlinearly realized Higgs sector formulated in Ref. [13]. In this nonlinear formalism, the effective Lagrangian below the cutoff scale Λ contains the Higgs field H transforming as a weak singlet, the would-be Goldstone boson field $\vec{\omega}$, and the electroweak gauge boson fields, and it respects the electroweak gauge symmetry, charge conjugation C and parity P , and the custodial $SU(2)_c$ symmetry. Up to dimension-4, the effective Lagrangian is given by [13]

$$\begin{aligned} \mathcal{L} = & -\frac{1}{4} \vec{W}_{\mu\nu} \cdot \vec{W}^{\mu\nu} - \frac{1}{4} B_{\mu\nu} B^{\mu\nu} \\ & + \frac{1}{4} (v^2 + 2\kappa v H + \kappa' H^2) \text{Tr}(D_\mu \Sigma^\dagger D^\mu \Sigma) \\ & + \frac{1}{2} \partial_\mu H \partial^\mu H - \frac{m_H^2}{2} H^2 - \frac{\lambda_3 v}{3!} H^3 + \frac{\lambda_4}{4!} H^4, \end{aligned} \quad (2)$$

where $\vec{W}_{\mu\nu}$ and $B_{\mu\nu}$ are field strengths of the electroweak gauge fields, $v \simeq 246$ GeV is the vacuum expectation value breaking the electroweak gauge symmetry, (κ, λ_3) and (κ', λ_4) are dimensionless coupling constants from the dimension-3 and dimension-4 operators, respectively. In Eq. (2), we have defined

$$\begin{aligned} \Sigma &= \exp\left(\frac{i\vec{\tau} \cdot \vec{\omega}}{v}\right), \\ D_\mu \Sigma &= \partial_\mu \Sigma + ig \frac{\vec{\tau}}{2} \cdot \vec{W}_\mu \Sigma - ig' B_\mu \Sigma \frac{\tau_3}{2}, \end{aligned} \quad (3)$$

in which the Pauli matrix τ_i is normalized as $\text{Tr}(\tau_i \tau_j) = 2\delta_{ij}$, and g and g' are the $SU(2)$ and $U(1)$ gauge coupling constants, respectively. The SM corresponds to $\kappa = \kappa' = 1$ and $\lambda_3 = \lambda_4 = \lambda = 3m_H^2/v^2$.

We note that at the tree level, only the dimension-3 operator $\frac{1}{2}\kappa v H D_\mu \Sigma^\dagger D^\mu \Sigma$ in Eq. (2) contains the anomalous HVV coupling that can contribute to the VV scatterings (cf. Fig. 1). Therefore, VV scatterings can test this dimensionless coupling κ , and $\Delta\kappa \equiv \kappa - 1$ measures the deviation from the SM value $\kappa = 1$.

B. Precision Constraints on the Coupling κ

Eq. (2) shows an important difference between the nonlinearly and the linearly realized Higgs sectors. The nonlinear formalism allows new physics to appear in the effective operators with dimension ≤ 4 whose coefficients are not necessarily suppressed by the cutoff scale Λ . Hence, the gauge couplings of Higgs boson to weak bosons can naturally deviate from the SM-values by an amount at the order of $\lesssim \mathcal{O}(1)$, as suggested by the naive dimensional analysis [23].

In the unitary gauge, the anomalous couplings of Higgs boson to gauge bosons relevant to the precision oblique parameters (S, T, U) [24] are:

$$\frac{[4(\kappa - 1)vH + 2(\kappa' - 1)H^2]}{v^2} \left[m_W^2 W_\mu^+ W^{-\mu} + \frac{1}{2} m_Z^2 Z_\mu Z^\mu \right].$$

When calculating radiative corrections using the effective Lagrangian (2), it is generally necessary to introduce higher dimensional counter terms to absorb the new divergences arising from the loop integration. There are in principle three next-to-leading order (NLO) counter terms to render the (S, T, U) parameters finite at the one-loop level, namely

$$\begin{aligned} \mathcal{L}^{(2)'} &= \ell_0 \frac{v^2}{16\pi^2} \frac{1}{4} [\text{Tr} \mathcal{T} (D_\mu \Sigma) \Sigma^\dagger]^2, \\ \mathcal{L}_1^{(4)} &= \ell_1 \frac{v^2}{\Lambda^2} gg' \text{Tr}[\mathbf{B}_{\mu\nu} \Sigma^\dagger \mathbf{W}^{\mu\nu} \Sigma], \\ \mathcal{L}_8^{(4)} &= \ell_8 \frac{v^2}{\Lambda^2} \frac{g^2}{4} [\text{Tr}(\mathcal{T} \mathbf{W}_{\mu\nu})]^2, \end{aligned} \quad (4)$$

whose coefficients (ℓ_0, ℓ_1, ℓ_8) correspond to the oblique parameters (T, S, U) , respectively. Here $\mathbf{W}_{\mu\nu} = \vec{W}_{\mu\nu} \cdot \vec{\tau}/2$, $\mathbf{B}_{\mu\nu} = B_{\mu\nu} \tau_3/2$, and $\mathcal{T} \equiv \Sigma \tau_3 \Sigma^\dagger$. Comparing to $\mathcal{L}_1^{(4)}$, $\mathcal{L}_8^{(4)}$ is of the same dimension, but with two new $SU(2)_c$ -violating operators \mathcal{T} , so that we expect $\ell_8/\ell_1 \sim 1/16\pi^2 \sim 10^{-2} \ll 1$. This generally leads to $U \ll S, T$. To estimate the contribution of loop corrections, we invoke a naturalness assumption that no fine-tuned accidental cancellation occurs between the leading logarithmic term and the constant piece of the counter terms. Thus, the leading logarithmic term represents a reasonable estimate of the loop corrections. This approach is commonly used in the literature for

estimating new physics effects in effective theories [26]. It is straightforward to compute the radiative corrections to S , T , and U , arising from the HVV anomalous couplings, using dimensional regularization in the $\overline{\text{MS}}$ scheme and keeping only the leading logarithmic terms. After subtracting the SM Higgs contributions ($\kappa = 1$) with the reference value m_H^{ref} , we find

$$\begin{aligned}\Delta S &= \frac{1}{6\pi} \left[\ln \frac{m_H}{m_H^{\text{ref}}} - (\kappa^2 - 1) \ln \frac{\Lambda}{m_H} \right], \\ \Delta T &= \frac{3}{8\pi c_w^2} \left[-\ln \frac{m_H}{m_H^{\text{ref}}} + (\kappa^2 - 1) \ln \frac{\Lambda}{m_H} \right], \\ \Delta U &= 0,\end{aligned}\tag{5}$$

where the terms containing $\ln \Lambda$ represent the genuine new physics effect arising from physics above the cut-off scale Λ [27]. Note that at the one-loop order, the coupling κ' has no contribution to the S , T and U parameters. In the SM ($\kappa = 1$), an increase of the Higgs mass will increase ΔS and decrease ΔT . Choosing the reference Higgs mass m_H^{ref} to be m_H , we may further simplify Eq. (5) as

$$\begin{aligned}\Delta S &= -\frac{\kappa^2 - 1}{6\pi} \ln \frac{\Lambda}{m_H}, \\ \Delta T &= +\frac{3(\kappa^2 - 1)}{8\pi c_w^2} \ln \frac{\Lambda}{m_H}, \\ \Delta U &= 0.\end{aligned}\tag{6}$$

For a given value of Λ and m_H , we find $\Delta S < 0$ and $\Delta T > 0$ for $|\kappa| > 1$. This pattern of radiative corrections allows a relatively heavy Higgs boson to be consistent with the current precision data [cf. Fig. 2(a)]. Furthermore, from Eq. (6) we see that the loop contribution from $\kappa \neq 1$ results in a sizable ratio of $\Delta T/\Delta S = -9/(4c_w^2) \approx -3$.

Within the framework of the SM, the global fit to the current precision electroweak data favors a light Higgs boson with a central value $m_H = 83$ GeV (significantly below the LEP2 direct search limit $m_H > 114.3$ GeV [28]) and a 95% C.L. limit, $32 \text{ GeV} \leq m_H \leq 192$ GeV, on the range of the Higgs boson mass. However, it was recently shown that in the presence of *new physics*, such a bound can be substantially relaxed [29–33]. The latest NuTeV data was not included in the above analysis. If we include the NuTeV data, the value of the minimum χ^2 of the global fit increases substantially (by 8.7), showing a poor quality of the SM fit to the precision data (this fit also gives a similar central value $m_H = 85$ GeV and 95% C.L. mass range $33 \text{ GeV} \leq m_H \leq 200$ GeV). We also find a similar increase of χ^2 (by 8.9) in the $\Delta S - \Delta T$ fits, which implies that the NuTeV anomaly may not be explained by new physics effect from the oblique parameters (ΔS , ΔT) alone. As the potential problems

with the NuTeV analysis are still under debate [34], we will not include the NuTeV data in the following analysis. [But for comparison, we have also displayed a 95% C.L. contour (dotted curve) from the fit including the NuTeV anomaly in Fig. 2(a).] In Fig. 2(a), we show the $\Delta S - \Delta T$ bounds (setting $m_H^{\text{ref}} = 100$ GeV) derived from the global fit with the newest updated electroweak precision data [35,36]. Furthermore, for $m_H^{\text{ref}} = 115$ (300) GeV and $\Delta U = 0$, we find that the global fit gives

$$\begin{aligned}\Delta S &= 0.01 (-0.07) \pm 0.09, \\ \Delta T &= 0.07 (0.16) \pm 0.11.\end{aligned}\tag{7}$$

In the same figure, we also plot the SM Higgs boson contributions to ΔS and ΔT with different Higgs masses. Fig. 2(b) shows that the upcoming measurements of the W^\pm mass (m_W) and top mass (m_t) at the Tevatron Run-2 can significantly improve the constraints on new physics via the oblique corrections, in which we have input the current Run-1 central values of (m_W , m_t) and the expected errors of (m_W and m_t) from the planned Run-2 sensitivity of 20 MeV and 2 GeV, respectively.

Using the allowed range of (ΔS , ΔT) in Fig. 2(a), we can further constrain the new physics scale Λ as a function of the anomalous coupling $\Delta\kappa$ for some typical values of $m_H^{\text{ref}} = m_H$ [cf. Eq. (6)]. Fig. 3 depicts these constraints. With Fig. 3, we can alternatively constrain the range of $\Delta\kappa$ for a given value of (Λ , m_H), which is summarized in Table I. Fig. 3 and Table I show that for $m_H \gtrsim 250 - 300$ GeV, the $\Delta\kappa < 0$ region is fully excluded, while a sizable $\Delta\kappa > 0$ is allowed so long as Λ is relatively low. Moreover, for $m_H \gtrsim 800$ GeV, the region $\Lambda < 1.1$ TeV is excluded. For the range of $m_H \gtrsim 250 - 300$ GeV, the preferred values of $\Delta\kappa > 0$ require the HW^+W^- and HZZ couplings to be stronger than those in the SM. In this case, the direct production rate of the Higgs boson, via either the Higgs-strahlung or the VV fusions in high energy collisions, should raise above the SM rate. On the other hand, for $m_H \lesssim 250$ GeV, the direct production rate of the Higgs boson can be smaller or larger than the SM rate depending on the sign of $\Delta\kappa$. Hence, when $\Delta\kappa < 0$, a light non-standard Higgs boson may be partially *hidden* by its large SM background events. However, in this situation, the new physics scale Λ will be generally low. For instance, when $m_H = 115$ GeV, a negative $\Delta\kappa = -0.15$ (-0.28) already forces $\Lambda \leq 1$ (0.4) TeV. Finally, we comment that, for a certain class of models, new physics effects may also be induced by extra heavy fermions such as in the typical top-seesaw models with new vector-like fermions [29,37] or models with new chiral families [31]. In these models, there can be generic positive con-

tributions to ΔT , so that the $\Delta\kappa < 0$ region may still be allowed for a relatively heavy Higgs boson, but such possibilities are very model-dependent. In our current effective theory analysis, we consider the bosonic HVV couplings as the dominant contributions to the oblique parameters, and assume that other possible anomalous couplings (such as the deviation in the gauge interactions of $tbW/t\bar{t}Z$ [38]) can be ignored. However, independent of these assumptions, the *most decisive test* of the HVV couplings can come from the direct measurements via Born-level processes at the high energy colliders, which is the subject of the next two sections.

C. Constraints on κ from Unitarity Requirement

Before concluding this section, we discuss the possibility of unitarity violation in the scattering process $pp \rightarrow W^+W^+jj \rightarrow \ell\nu\ell\nu jj$ for $\kappa \neq 1$, whose leading contribution comes from the sub-process $W_L^+W_L^+ \rightarrow W_L^+W_L^+$ when the initial W_L^+ bosons are almost collinearly radiated from the incoming quarks or antiquarks. The scattering amplitude of $W_L^+W_L^+ \rightarrow W_L^+W_L^+$ contributes to the isospin $I = 2$ channel, and in the high energy region ($E^2 \gg m_W^2, m_H^2$), it is dominated by the leading E^2 -contributions, and

$$T[I = 2] \simeq (\kappa^2 - 1) \frac{E^2}{v^2}. \quad (8)$$

Using the partial-wave analysis, the s -wave amplitude $a_{I,J=2,0}$ is found to be

$$a_{20} \simeq (\kappa^2 - 1) \frac{E^2}{16\pi v^2}, \quad (9)$$

where $E = M_{VV}$ is the invariant mass of the vector boson pair. The unitarity condition for this channel is¹ $|\text{Re } a_{20}| < 2!/2 = 1$, in which the factor $2!$ is due to the identical particles (W^+W^+) in the final state. This results in a requirement that

$$\sqrt{1 - \frac{16\pi v^2}{E^2}} < |\kappa| < \sqrt{1 + \frac{16\pi v^2}{E^2}}. \quad (10)$$

For example,

$$\begin{aligned} |\kappa| < 3.6, & \quad \text{for } E = 0.5 \text{ TeV,} \\ 0.5 < |\kappa| < 1.3, & \quad \text{for } E = 2 \text{ TeV,} \\ 0.8 < |\kappa| < 1.2, & \quad \text{for } E = 3 \text{ TeV.} \end{aligned} \quad (11)$$

¹Another convention in the literature [16,17] reads, $|\text{Re } a_{20}| < 1/2$, for $a_{20} \simeq (\kappa^2 - 1)E^2/(32\pi v^2)$. In this convention, the partial wave amplitude of the elastic scattering $W^+W^+ \rightarrow W^+W^+$, beyond the tree level, satisfies the relation $\text{Im } a = |a|^2$.

As to be shown in the next section, the expected sensitivity of the LHC to determining $\Delta\kappa$ [cf. Eq. (13)] is consistent with the unitarity limit since the typical invariant mass of the W^+W^+ pair, after the kinematic cuts, falls into the range $500 \text{ GeV} \leq E \leq 2 \sim 3 \text{ TeV}$. The contributions from higher invariant mass values are severely suppressed by parton luminosities [17,39], and are thus negligible.

IV. TESTING κ VIA VV SCATTERINGS AT THE LHC

Knowing the above constraints, we turn to the analysis of testing κ via VV scatterings at the LHC. Following the procedures described in Sec. II, we calculate the tree-level cross sections of the scattering processes

$$\begin{aligned} pp &\rightarrow Z_L Z_L jj \rightarrow \ell^+ \ell^- \ell^+ \ell^- jj, \ell^+ \ell^- \nu \bar{\nu} jj, \\ pp &\rightarrow W_L^+ W_L^- jj \rightarrow \ell^+ \nu \ell^- \bar{\nu} jj, \\ pp &\rightarrow W_L^+ W_L^+ jj \rightarrow \ell^+ \nu \ell^+ \nu jj, \\ pp &\rightarrow W_L^- W_L^- jj \rightarrow \ell^- \bar{\nu} \ell^- \bar{\nu} jj, \\ pp &\rightarrow Z_L W_L^+ jj \rightarrow \ell^+ \ell^- \ell^+ \nu jj, \\ pp &\rightarrow Z_L W_L^- jj \rightarrow \ell^+ \ell^- \ell^- \bar{\nu} jj. \end{aligned} \quad (12)$$

In our numerical calculations, we shall take the same kinematic cuts as those proposed in Ref. [17] to suppress the backgrounds discussed in Sec. II. It has been shown in the Table II of Ref. [17] that, after imposing the kinematical cuts, the sum of the cross sections of the QCD background and the top quark background is smaller than the cross section of the remaining electroweak background by one order of magnitude. Thus, the EW background needs to be studied in more detail. For that, we have examined the polarization of the final state W^+ bosons. In Table II, we list the cross section of $pp \rightarrow W_{\lambda_1}^+ W_{\lambda_2}^+ jj$ at the LHC, for various values of $\Delta\kappa$ with $m_H = 115 \text{ GeV}$, where W_λ^+ denotes a polarized W boson with the polarization index $\lambda = T$ or L . As expected, when $|\Delta\kappa|$ is large, the $W_L^+ W_L^+$ production rate dominates, and all the SM backgrounds, after the kinematical cuts, are reasonably suppressed relative to the signal due to the E^2 -dependence of the $W_L W_L$ amplitude. However, for $\Delta\kappa = 0$ (the SM case), although the QCD and top quark backgrounds are negligibly small, the EW background contributed from the TT and LT polarizations are still quite large as compared to the signal, cf. Table II. Therefore, in this work, we shall take the cross section for $\Delta\kappa = 0$ (the SM case) as the remaining EW background cross section.

In Tables III–VI, we list the obtained numbers of events (including both the signals and backgrounds)

for an integrated luminosity of 300 fb^{-1} with the parameters $115 \text{ GeV} \leq m_H \leq 300 \text{ GeV}$ and $-1.0 \leq \Delta\kappa \leq 0.7$. In general, the number of events for $\kappa > 0$ and $\kappa < 0$ are not the same. However, the result of our calculations shows that the difference between them is very small. Thus, we only list the number of events with $\Delta\kappa \geq -1$ ($\kappa \geq 0$) in the Tables. We see that the most sensitive channel to determine the anomalous coupling $\Delta\kappa$ is $pp \rightarrow W^+W^+jj \rightarrow l^+\nu l^+\nu jj$ (cf. Table III) due to its small background rates, and thus the weakest kinematic cuts [17].

It is easy to check that the numbers in Tables V and VI, for the ZW^\pm and ZZ channels, are consistent with the unitarity bound. Only the W^+W^- channel, cf. Table IV, needs further unitarization [16,17]. It is expected that after unitarizing the scattering amplitudes, the corresponding numbers in Table IV will become smaller, and thus this channel is less interesting. Therefore, in this paper we only take the best channel, the W^+W^+ channel (cf. Table III), to constrain $\Delta\kappa$.

As discussed above, we shall take the SM events (for $\Delta\kappa = 0$) listed in Table III as the intrinsic SM electroweak background rate in our analysis, i.e., $N_B \equiv N(\Delta\kappa = 0)$. We can then define the number of signal events (for $\Delta\kappa \neq 0$) as $N_S \equiv N(\Delta\kappa \neq 0) - N_B$. The total statistical fluctuation is $\sqrt{N_S + N_B}$. To study the potential of the LHC in distinguishing the $\Delta\kappa \neq 0$ case from the SM, we also show the deviation of the signal from the total statistical fluctuation, $N_S/\sqrt{N_S + N_B}$, in the parentheses in Tables III. The values of $N_S/\sqrt{N_S + N_B}$ in Table III show that the LHC can limit $\Delta\kappa$ to the range

$$-0.3 < \Delta\kappa < 0.2 \quad (13)$$

at roughly $(1 - 3)\sigma$ level if no anomalous coupling ($\Delta\kappa \neq 0$) effect is detected.

As mentioned in Sec. I, if the new physics above the cutoff scale Λ happens to make $\Delta\kappa$ negative and close to $\Delta\kappa = -1$ ($\kappa \gtrsim 0$), the Higgs production rate may become so small that the Higgs resonance may be difficult to detect. However, we see from Tables III that the event numbers of $pp \rightarrow W^+W^+jj \rightarrow l^+\nu l^+\nu jj$ for this κ value are much larger than those for the SM, so that we can clearly detect the $\kappa \gtrsim 0$ effect via these processes without the need of detecting the resonance of a light Higgs boson. This is the clear advantage of this type of measurements when the resonant state of the Higgs boson is difficult to be directly detected experimentally.

V. OTHER POSSIBLE TESTS OF κ FROM FUTURE COLLIDER EXPERIMENTS

There can be other tests of κ from future collider experiments. After discussing a few relevant measurements available at the Fermilab Tevatron and the CERN LHC, we shall also comment on the potential of the future LC. They are given below in order.

A. Associate HV Production

First, let us consider the associate production of Higgs boson and vector boson ($H + V$) at high energy colliders. The studies at LEP-2 concluded that the mass of the SM Higgs boson has to be larger than about 114.3 GeV [28]. For a non-SM Higgs boson, this lower mass bound will be different. For example, in the supersymmetric SM, the H - Z - Z coupling is smaller than that of the SM by a factor of $\sin(\alpha - \beta)$ or $\cos(\alpha - \beta)$, depending whether H denotes a light or a heavy CP-even Higgs boson, and the above-mentioned lower mass bound is reduced to about 90 GeV [40]. If the mass of the SM Higgs boson is around 110 GeV , it can be discovered at the Tevatron Run-2. Assuming an integrated luminosity of 10 fb^{-1} , the number of the expected signal events is about 27 and the background events about 258, according to the Table 3 (the most optimal scenario) of Ref. [41]. Therefore, the one sigma statistic fluctuation of the total event is $\sqrt{27 + 258} \sim 17$. Consequently, at the 1σ level, $0.6 < |\kappa| < 1.2$, and at the 2σ level, $|\kappa| < 1.5$.² Similarly, we estimate the bounds on $|\kappa|$ for various m_H as follows:

| $m_H(\text{GeV})$ | 1σ | 2σ |
|-------------------|-------------------------------|-----------------------------|
| 110 : | $0.6 \leq \kappa \leq 1.2,$ | $0 \leq \kappa \leq 1.5,$ |
| 120 : | $0.4 \leq \kappa \leq 1.4,$ | $0 \leq \kappa \leq 1.6,$ |
| 130 : | $0 \leq \kappa \leq 1.5,$ | $0 \leq \kappa \leq 1.8,$ |

We see that the above limits on κ are weaker than that in Eq. (13). Of course, the above bounds can be further improved at the Tevatron Run-2 by having a larger integrated luminosity until the systematical error dominates the statistical error. The same process can also be studied at the LHC to test the anomalous coupling κ . However, because of the much larger background rates at the LHC, the improvement on the measurement of κ via the associate production of V and Higgs boson is not expected to be significant.

²This bound can be improved by carefully examining the invariant mass distribution of the $b\bar{b}$ pairs.

B. Measuring Total Decay Width of Higgs Boson

The anomalous HVV coupling can also be tested from measuring the total decay width of the Higgs boson. When the Higgs boson mass is larger than twice of the Z boson mass, it can decay into a Z boson pair which subsequently decay into 4 muons. This decay channel is labelled as one of the “gold-plated” channels (the pure leptonic decay modes) because it is possible to construct the invariant mass of the ZZ pair in this decay mode with a high precision, which provides a precision measurement on the total decay width of the Higgs boson. A detailed Monte Carlo analysis has been carried out in Ref. [42] to find out the uncertainty on the measurement of the Higgs boson width. Assuming that there is no non-SM decay channel opened and only the anomalous HVV coupling is important, one can convert the conclusion from [42] to the bounds on $\Delta\kappa$. Since the decay branching ratio of $H \rightarrow W^+W^-$ or ZZ for a SM heavy Higgs boson is large (almost one hundred percent for $m_H > 300$ GeV), the total width measurement can give a strong constraint on κ . We define the accuracy on the determination of κ using the relation $-n\Delta\Gamma \leq \Gamma(\kappa) - \Gamma(\kappa = 1) \leq n\Delta\Gamma$, where $n = 1, 2$ denoting the 1σ and 2σ accuracy, respectively, and $\Gamma(\kappa)$ is the width of the Higgs boson for a general value of κ , $\Gamma(\kappa = 1)$ is for a SM Higgs boson and $\Delta\Gamma$ is the experimental accuracy in measuring the Higgs boson width. From the Table 3 of Ref. [42], we find that at the LHC (with an integrated luminosity of 300 fb^{-1} [43]), the bounds on $\Delta\kappa$ obtained from the measurement of the total decay width of Higgs boson, via the process $pp \rightarrow H \rightarrow ZZ \rightarrow \mu^+\mu^-\mu^+\mu^-$, are as follows:

| $m_H(\text{GeV})$ | 1σ | 2σ |
|-------------------|-------------------------------|-------------------------------|
| 200 – 300 : | $0.9 \leq \kappa \leq 1.1,$ | $0.8 \leq \kappa \leq 1.2.$ |

(15)

C. Decay Branching Ratio of $H \rightarrow \gamma\gamma$

Another important effect of a non-vanishing anomalous coupling κ is to modify the decay branching ratio of $H \rightarrow \gamma\gamma$, and hence, the production rate of $gg \rightarrow H \rightarrow \gamma\gamma$ at the LHC. In Table VII, we list the decay branching ratio $B(H \rightarrow \gamma\gamma)$ as a function of $\Delta\kappa$ for various m_H . As shown, $B(H \rightarrow \gamma\gamma)$ decreases for $\Delta\kappa > 0$, and increases for $\Delta\kappa < 0$. For example, for a 120 GeV Higgs boson, $B(H \rightarrow \gamma\gamma)$ decreases by 14% for $\Delta\kappa = 0.2$ and increases by 45% for $\Delta\kappa = -0.3$.

D. Detecting a Higgs Boson Resonance

When the SM Higgs boson is light, it is expected that the production rate of $qq \rightarrow qqH$ with $H \rightarrow WW^* \rightarrow \ell\ell\cancel{E}_T$ is large enough to be detected at the LHC, and this process can also be used to test the coupling of the HWW [44] by studying the observables near the Higgs boson resonance. In the effective Lagrangian (2), the Lorentz structure (and the dimension) of the anomalous couplings κ and κ' is the same as the SM coupling. Therefore, the result of the study performed in Ref. [44] also holds for the current study when m_H is less than twice of the Z boson mass. In this case, its production rate is $\kappa^2\mathcal{S}_{SM}B(\kappa)/B(\kappa = 1)$, where \mathcal{S}_{SM} is the SM rate, and $B(\kappa)$ is the decay branching ratio of $H \rightarrow WW^*$ for a general value of κ . Needless to say that $B(\kappa = 1)$ corresponds to the SM branching ratio.

When the WW (and ZZ) decay mode dominates the Higgs boson decay, such as when m_H is larger than twice of W boson mass, the ratio of the decay branching ratios for $H \rightarrow WW^*$, $B(\kappa)/B(\kappa = 1)$, would be close to 1. However, this ratio can be quite different from 1 when m_H is small. For example, for $m_H = 120$ GeV, the ratio $B(\kappa)/B(\kappa = 1)$ is 0.68 and 1.4, respectively, for $\kappa = 0.8$ and $\kappa = 1.2$. From the Table 1 of Ref. [44], one can determine the constraint on the ratio $\kappa^2B(\kappa)/B(\kappa = 1)$, denoted as R , using the relation $\mathcal{S}_{SM} - n\sqrt{\mathcal{B} + \mathcal{S}_{SM}} \leq R\mathcal{S}_{SM} \leq \mathcal{S}_{SM} + n\sqrt{\mathcal{B} + \mathcal{S}_{SM}}$, where \mathcal{B} is the background rate and $n = 1, 2$ denotes the 1σ and 2σ accuracy, respectively. Assuming an integrated luminosity of 300 fb^{-1} , we find that the bounds on R for various m_H are:

| m_H (GeV) | 1σ | 2σ |
|-------------|--------------------------|--------------------------|
| 110 : | $0.87 \leq R \leq 1.13,$ | $0.74 \leq R \leq 1.26,$ |
| 120 : | $0.94 \leq R \leq 1.06,$ | $0.88 \leq R \leq 1.12,$ |
| 130 : | $0.97 \leq R \leq 1.03,$ | $0.93 \leq R \leq 1.07,$ |
| 150 : | $0.97 \leq R \leq 1.03,$ | $0.94 \leq R \leq 1.06,$ |
| 170 : | $0.98 \leq R \leq 1.02,$ | $0.95 \leq R \leq 1.05.$ |

(16)

To extract the bound on κ , we need to know the decay branching ratio $B(\kappa)$ of $H \rightarrow WW^*$ assuming that the effective Lagrangian (2) differs from the SM Lagrangian only in the coefficient κ . A few values of $B(\kappa)$ as a function of κ for various m_H are given in Table VIII. The result of Table VIII and Eq. (16) indicate that κ can be measured at a few percent level when a light Higgs boson is detected. However, in our opinion, this conclusion seems to be too optimistic because the systematical error of the experiment at the LHC is expected to be at the similar level of accuracy.

E. At Linear Collider

Before closing this section, we note that the anomalous coupling of HZZ and HW^+W^- can also be tested at the LC via the processes $e^-e^+ \rightarrow ZH(\rightarrow b\bar{b})$, $e^-e^+ \rightarrow e^-e^+H(\rightarrow b\bar{b})$ via ZZ fusion, and $e^-e^+ \rightarrow \nu\bar{\nu}H(\rightarrow b\bar{b})$ via W^+W^- fusion. In Refs. [3,4], it was concluded that $\Delta\kappa$ can be determined better than a percent level for a 120 GeV SM-like Higgs boson produced from the above processes, assuming an integrated luminosity of 1 ab^{-1} for a 500 GeV (or 800 GeV) LC. After converting the notation in Ref. [4] to ours, the 2σ error in measuring $\Delta\kappa$ is found to be at the level of 0.3%. Thus, the expected precision in the measurement of $\Delta\kappa$ at a high luminosity LC is higher than that at the LHC, in the case of a SM-like Higgs boson (i.e., the decay branching ratio of $H \rightarrow b\bar{b}$ is about 1). Even in the case that the Higgs boson is not SM-like, the LC can still determine $\Delta\kappa$ by studying the Higgs-strahlung process $e^-e^+ \rightarrow Z(\rightarrow \ell^+\ell^-)H$ and ZZ fusion process $e^-e^+ \rightarrow e^-e^+H$, where H decays into anything [5]. However, due to its much smaller rate, the sensitivity to $\Delta\kappa$ is lower than the SM-like case. In the next section, we shall show that the precision of determining the dimension-6 anomalous couplings via VV scatterings at the LHC will be comparable to the level of the precision expected at the LC.

VI. TESTING ANOMALOUS HVV COUPLINGS FROM DIMENSION-6 OPERATORS

A. Anomalous HVV Couplings from Dimension-6 Operators

Now we consider the test of the anomalous HVV couplings from the dimension-6 operators arising from the linearly realized effective Lagrangian. In the linearly realized effective Lagrangian, there is no gauge invariant anomalous operators at dimension-3 and dimension-4, and the leading anomalous HVV couplings are from the effective operators of dimension-6 [14,15]. (All the gauge invariant operators with dimension 4 or less have been included in the SM Lagrangian.) In the following, we shall analyze the test of these leading order anomalous couplings. As is shown in Refs. [14,15], the C and P conserving effective Lagrangian up to dimension-6 operators containing a Higgs doublet Φ and the weak bosons V^a is given by

$$\mathcal{L}_{\text{eff}} = \sum_n \frac{f_n}{\Lambda^2} \mathcal{O}_n, \quad (17)$$

where f_n 's are the anomalous coupling constants. The operators \mathcal{O}_n 's are [14,15]

$$\begin{aligned} \mathcal{O}_{\Phi,1} &= (D_\mu \Phi)^\dagger \Phi^\dagger \Phi (D^\mu \Phi), \\ \mathcal{O}_{BW} &= \Phi^\dagger \hat{B}_{\mu\nu} \hat{W}^{\mu\nu} \Phi, \\ \mathcal{O}_{DW} &= \text{Tr} \left(\left[D_\mu, \hat{W}_{\nu\rho} \right] \left[D^\mu, \hat{W}^{\nu\rho} \right] \right), \\ \mathcal{O}_{DB} &= -\frac{g'^2}{2} (\partial_\mu B_{\nu\rho}) (\partial^\mu B^{\nu\rho}), \\ \mathcal{O}_{\Phi,2} &= \frac{1}{2} \partial^\mu (\Phi^\dagger \Phi) \partial_\mu (\Phi^\dagger \Phi), \\ \mathcal{O}_{\Phi,3} &= \frac{1}{3} (\Phi^\dagger \Phi)^3, \\ \mathcal{O}_{WWW} &= \text{Tr} [\hat{W}_{\mu\nu} \hat{W}^{\nu\rho} \hat{W}_\rho^\mu], \\ \mathcal{O}_{WW} &= \Phi^\dagger \hat{W}_{\mu\nu} \hat{W}^{\mu\nu} \Phi, \\ \mathcal{O}_{BB} &= \Phi^\dagger \hat{B}_{\mu\nu} \hat{B}^{\mu\nu} \Phi, \\ \mathcal{O}_W &= (D_\mu \Phi)^\dagger \hat{W}^{\mu\nu} (D_\nu \Phi), \\ \mathcal{O}_B &= (D_\mu \Phi)^\dagger \hat{B}^{\mu\nu} (D_\nu \Phi), \end{aligned} \quad (18)$$

where $\hat{B}_{\mu\nu}$ and $\hat{W}_{\mu\nu}$ stand for

$$\hat{B}_{\mu\nu} = i \frac{g'}{2} B_{\mu\nu}, \quad \hat{W}_{\mu\nu} = i \frac{g}{2} \sigma^a W_{\mu\nu}^a, \quad (19)$$

in which g and g' are the $SU(2)$ and $U(1)$ gauge coupling constants, respectively.

At tree level, the operators $\mathcal{O}_{\Phi,1}$, \mathcal{O}_{BW} , \mathcal{O}_{DW} and \mathcal{O}_{DB} in Eq. (18) affect the two-point functions of the weak boson V when Φ is taken to be its vacuum expectation value:

$$\Phi \rightarrow \frac{1}{\sqrt{2}} \begin{pmatrix} 0 \\ v \end{pmatrix}. \quad (20)$$

Thus, they are severely constrained by the precision Z -pole and low energy data. In Ref. [15], it was concluded that at the 95% level, in unites of TeV^{-2} , the magnitude of $\frac{f_{DW}}{\Lambda^2}$ or $\frac{f_{\Phi,1}}{\Lambda^2}$ is constrained to be less than 1, and $\frac{f_{DB}}{\Lambda^2}$ or $\frac{f_{BW}}{\Lambda^2}$ can be about a factor of 10 larger. We shall update these bounds in Sec. VI.B. Since it will be very difficult to observe the effect of these operators in the high-energy observables, in what follows, we will neglect their effect when discussing the VV scatterings.

The two operators $\mathcal{O}_{\Phi,1}$ and $\mathcal{O}_{\Phi,2}$ in Eq. (18) lead to a finite renormalization of the Higgs boson wave function [15]. Similarly, the two operator $\mathcal{O}_{\Phi,3}$ induces a finite renormalization of the Higgs potential [15]. In a recent paper [4], it was shown that after renormalizing the Higgs boson field so that the residue of its propagator at its mass pole is equal to one, two effective anomalous couplings of Higgs boson to gauge bosons are induced by the dimension-6 operator $\mathcal{O}_{\Phi,2}$ as

$$\frac{-f_{\Phi,2}(vH + H^2)}{\Lambda^2} \left[m_W^2 W_\mu^+ W^{-\mu} + \frac{1}{2} m_Z^2 Z_\mu Z^\mu \right].$$

After converting the above anomalous couplings to the notation introduced in Sec. III for a non-linear effective theory, the anomalous coupling $\Delta\kappa$ corresponds to $\frac{-f_{\Phi,2}v^2}{4\Lambda^2}$. For example, at a 500 GeV (or 800 GeV) LC with an integrated luminosity of 1 ab^{-1} , the 2σ statistical error on the determination of the anomalous coupling $\frac{f_{\Phi,2}}{\Lambda^2}$ is at the level of 0.2 TeV^{-2} , for a 120 GeV SM-like Higgs boson [4]. This corresponds to the determination of $\Delta\kappa$ at about the 0.3% level. Since this operator can only generate E^2 -dependence of the $V_L V_L \rightarrow V_L V_L$ scattering amplitude, and it is best determined at the LC for a SM-like Higgs boson, in what follows, we will neglect its effect in our studies.

The operator \mathcal{O}_{WW} contributes to the triple and quartic vector boson self-couplings, but not the anomalous coupling of Higgs boson to gauge bosons. On the other hand, the last four operators \mathcal{O}_{WW} , \mathcal{O}_{BB} , \mathcal{O}_W and \mathcal{O}_B in Eq. (18) contribute to the following anomalous HVV couplings [15]:

$$\begin{aligned} \mathcal{L}_{\text{eff}}^H &= g_{H\gamma\gamma} H A_{\mu\nu} A^{\mu\nu} + g_{HZ\gamma}^{(1)} A_{\mu\nu} Z^\mu \partial^\nu H \\ &+ g_{HZ\gamma}^{(2)} H A_{\mu\nu} Z^{\mu\nu} + g_{HZZ}^{(1)} Z_{\mu\nu} Z^\mu \partial^\nu H \\ &+ g_{HZZ}^{(2)} H Z_{\mu\nu} Z^{\mu\nu} + g_{HWW}^{(1)} (W_{\mu\nu}^+ W^{-\mu} \partial^\nu H + \text{h.c.}) \\ &+ g_{HWW}^{(2)} H W_{\mu\nu}^+ W^{-\mu\nu}, \end{aligned} \quad (21)$$

where

$$\begin{aligned} g_{H\gamma\gamma} &= -\left(\frac{gm_W}{\Lambda^2}\right) \frac{s^2(f_{BB} + f_{WW})}{2}, \\ g_{HZ\gamma}^{(1)} &= \left(\frac{gm_W}{\Lambda^2}\right) \frac{s(f_W - f_B)}{2c}, \\ g_{HZ\gamma}^{(2)} &= \left(\frac{gm_W}{\Lambda^2}\right) \frac{s[s^2 f_{BB} - c^2 f_{WW}]}{c}, \\ g_{HZZ}^{(1)} &= \left(\frac{gm_W}{\Lambda^2}\right) \frac{c^2 f_W + s^2 f_B}{2c^2}, \\ g_{HZZ}^{(2)} &= -\left(\frac{gm_W}{\Lambda^2}\right) \frac{s^4 f_{BB} + c^4 f_{WW}}{2c^2}, \\ g_{HWW}^{(1)} &= \left(\frac{gm_W}{\Lambda^2}\right) \frac{f_W}{2}, \\ g_{HWW}^{(2)} &= -\left(\frac{gm_W}{\Lambda^2}\right) f_{WW}, \end{aligned} \quad (22)$$

with $s \equiv \sin\theta_W$, $c \equiv \cos\theta_W$. In our calculation, we have included the complete gauge invariant set of Feynman diagrams that receive contribution from the anomalous operators \mathcal{O}_{WWW} , \mathcal{O}_{WW} , \mathcal{O}_{BB} , \mathcal{O}_W and \mathcal{O}_B . For example, the triple vector boson self-couplings include the contributions from the operators \mathcal{O}_{WWW} , \mathcal{O}_W and \mathcal{O}_B , while the quartic vector boson self-couplings are induced by \mathcal{O}_{WWW} and \mathcal{O}_W . The reason that the operators \mathcal{O}_{WW} and \mathcal{O}_{BB} do not modify the gauge boson self-couplings is as

follow. When the Higgs field of those operators is replaced by its vacuum expectation value, it seems that they would induce anomalous operators to modify the gauge boson self-couplings. However, the resulting operators are proportional to the kinematic term of the $SU(2)$ and $U(1)$ gauge bosons, and lead to a finite wavefunction renormalization of the gauge fields by constants $Z_{2W}^{1/2} = (1 - g^2 f_{WW} v^2 / 2\Lambda^2)^{-1/2}$ and $Z_{2B}^{1/2} = (1 - g'^2 f_{BB} v^2 / 2\Lambda^2)^{-1/2}$, respectively. Therefore, from the fact that the building blocks of the effective Lagrangian \mathcal{L}_{eff} , cf. Eq. (17), involving gauge bosons are $gW_{\mu\nu}$, $g'B_{\mu\nu}$, and the covariant derivative D_μ , we can perform a finite charge renormalization of the gauge couplings g and g' by constants $Z_g = (1 + g^2 f_{WW} v^2 / 2\Lambda^2)^{-1/2}$ and $Z_{g'} = (1 + g'^2 f_{BB} v^2 / 2\Lambda^2)^{-1/2}$, respectively, so that the net effect of the operators \mathcal{O}_{WW} and \mathcal{O}_{BB} is to modify only the couplings of Higgs boson to gauge bosons, but not the self-couplings of gauge bosons.

In Eq. (21), the anomalous HVV couplings are expressed in terms of the Lorentz-invariant dimension-5 operators containing the Higgs boson and the gauge bosons W^\pm , Z and γ . Among them, the operators $HA_{\mu\nu} A^{\mu\nu}$, $HA_{\mu\nu} Z^{\mu\nu}$, $HZ_{\mu\nu} Z^{\mu\nu}$ and $HW_{\mu\nu}^+ W^{-\mu\nu}$ can also be induced from the gauge-invariant dimension-5 operators in the nonlinear realization of the Higgs sector because in which the Higgs field H is an electroweak singlet. Thus, it is worth noticing that the following LHC study of testing the linearly realized anomalous HVV couplings via VV scatterings may be generalized to the case of the dimension-5 operators in the nonlinear realization.

B. Constraints on f_n from the Existing Experiments and the Unitarity Requirement

There are known experiments that can constrain the size of the anomalous coupling constants f_n .

The constraints on the anomalous coupling constants f_{WWW} , f_{WW} , f_{BB} , f_W and f_B have been studied in Refs. [15,45,46]. At tree level, ΔS and ΔT are proportional to f_{BW}/Λ^2 and $f_{\Phi,1}/\Lambda^2$, respectively. Thus we can obtain the 68% and 95% CL bounds on the (f_{BW}/Λ^2) - $(f_{\Phi,1}/\Lambda^2)$ plane directly from the corresponding bounds in Fig. 2(a). This is shown in Fig. 4. We see from Fig. 4 that the precision data give quite strong constraints on f_{BW}/Λ^2 and $f_{\Phi,1}/\Lambda^2$. At one loop level, ΔS and ΔT are related to other five anomalous coupling constants through loop corrections. Following Refs. [15,45,46], we make a one parameter fit of the five anomalous coupling constants by using the formulas given in Ref. [46] and the updated ΔS - ΔT bounds in Fig. 2(a). The obtained 95%

CL constraints (in units of TeV^{-2}) for $m_H = 100$ GeV are:

$$\begin{aligned}
-6 &\leq f_{WWW}/\Lambda^2 \leq 3, \\
-6 &\leq f_W/\Lambda^2 \leq 5, \\
-4.2 &\leq f_B/\Lambda^2 \leq 2.0, \\
-5.0 &\leq f_{WW}/\Lambda^2 \leq 5.6, \\
-17 &\leq f_{BB}/\Lambda^2 \leq 20.
\end{aligned} \tag{23}$$

These constraints are much weaker than that shown in Fig. 4 because these five anomalous coupling constants contribute to ΔS and ΔT through one loop corrections which are suppressed by the loop factor $1/16\pi^2$.

The triple gauge coupling data lead to the following 95% CL constraints (in units of TeV^{-2}) [6,15,47,48]:

$$\begin{aligned}
-31 &\leq (f_W + f_B)/\Lambda^2 \leq 68 \quad \text{for } f_{WWW} = 0, \\
-41 &\leq f_{WWW}/\Lambda^2 \leq 26 \quad \text{for } f_W + f_B = 0.
\end{aligned} \tag{24}$$

Furthermore, the Higgs searches data at the LEP2 and the Tevatron can give rise to the following 95% CL bound on $f_{WW(BB)}$ (in units of TeV^{-2}) for $m_H \leq 150$ GeV [6]

$$-7.5 \leq \frac{f_{WW(BB)}}{\Lambda^2} \leq 18. \tag{25}$$

The theoretical constraint on f_n coming from the requirement of the unitarity of the S -matrix has been studied in Ref. [49]. In terms of the present symbols of the anomalous coupling constants, the unitarity bounds given in Ref. [49] read (in units of TeV^{-2})

$$\begin{aligned}
\left| \frac{f_B}{\Lambda^2} \right| &\leq \frac{98}{\Lambda^2}, & \left| \frac{f_W}{\Lambda^2} \right| &\leq \frac{31}{\Lambda^2}, \\
-\frac{784}{\Lambda^2} + \frac{3556m_W}{\Lambda^3} &\leq \frac{f_{BB}}{\Lambda^2} \leq \frac{638}{\Lambda^2} + \frac{3733m_W}{\Lambda^3}, \\
\left| \frac{f_{WW}}{\Lambda^2} \right| &\leq \frac{35.2}{\Lambda^2} + \frac{4.86}{\Lambda m_W}, & \left| \frac{f_{WWW}}{\Lambda^2} \right| &\leq \frac{38}{3g^2\Lambda^2},
\end{aligned} \tag{26}$$

in which we have put the center-of-mass energy $\sqrt{s} \approx \Lambda$. For $\Lambda \approx 2$ TeV, the bounds are (in units of TeV^{-2})

$$\begin{aligned}
\left| \frac{f_B}{\Lambda^2} \right| &\leq 24.5 & \left| \frac{f_W}{\Lambda^2} \right| &\leq 7.8 & \left| \frac{f_{WWW}}{\Lambda^2} \right| &\leq 7.5, \\
-160 &\leq \frac{f_{BB}}{\Lambda^2} \leq 197, & \left| \frac{f_{WW}}{\Lambda^2} \right| &\leq 39.2.
\end{aligned} \tag{27}$$

These bounds are essentially of the same level as the above bounds (23) and (24).

We see that, except for the constraints from the precision data (cf. Fig. 4), all other constraints are rather weak. Furthermore, the above constraints on f_n/Λ^2 lead to the following constraints (in units of TeV^{-1}) on the anomalous coupling constants $g_{HWW}^{(1)}$, $g_{HWW}^{(2)}$, $g_{HZZ}^{(1)}$ and $g_{HZZ}^{(2)}$, cf. Eq. (22), related to the VV scatterings:

$$\begin{aligned}
-0.20 &\leq g_{HWW}^{(1)} \leq 0.065, \\
-1.2 &\leq -g_{HWW}^{(2)} \leq 0.73, \\
-0.26 &\leq g_{HZZ}^{(1)} \leq 0.24, \\
-0.62 &\leq -g_{HZZ}^{(2)} \leq 0.36.
\end{aligned} \tag{28}$$

We shall see in the following subsection that the limits on these coupling constants obtained from studying the VV scattering processes at the LHC will be significantly stronger than those in Eq. (28).

C. Testing f_n via VV Scatterings at the LHC

The test of the anomalous HVV couplings from the dimension-6 operators via VV scatterings is quite different from that for the dimension-3 operator. The relevant operators in Eq. (18) contain two derivatives, so that the interaction vertices themselves behave as E^2 at high energies. Thus, at high energies, the scattering amplitudes of $V_L V_L \rightarrow V_L V_L$ grows as E^4 , and those containing transverse components, i.e., $V_T V_T \rightarrow V_L V_L$, $V_T V_L \rightarrow V_T V_L$ and $V_L V_L \rightarrow V_T V_T$, grow as E^2 . Hence, the scattering processes containing V_T actually behave as *signals* rather than backgrounds. This is very different from the case of the nonlinearly realized dim-3 anomalous coupling studied in Sec. IV. As discussed in Sec. II, since the $V_T V_T$ and $V_L V_T$ scatterings also contribute to the signal rate, we decide to do the full $2 \rightarrow 4$ tree level calculation, in contrast to performing the calculation using the EWA folded by the $2 \rightarrow 2$ VV scattering amplitudes. Nevertheless, we shall use the EWA to check the high energy behavior of the full calculation, in the case that the anomalous coupling is large.

We calculate the tree level cross sections for all the processes listed in Eq. (12) with the same method described in Sec. IV, but for the linearly realized effective Lagrangian theory. Since there are several dim-6 anomalous couplings related to the VV scatterings in this theory [cf. Eq. (18)], the analysis is more complicated than in the nonlinear realization case. If the anomalous coupling constants are of the same order of magnitude, the interferences between them may be significant, depending on the relative phases among them. This undoubtedly complicates the analysis. In

the following, we again perform the single parameter analysis, i.e., assuming only one of the anomalous coupling constants is dominant at a time. We see from Eq. (18) that the coupling constants related to VV scatterings are f_{WWW} , f_{WW} , f_{BB} , f_W and f_B . As discussed in Sec. VI.A, the operator \mathcal{O}_{WWW} does not induce the anomalous coupling of Higgs boson to gauge bosons, and it may not be directly related to the electroweak symmetry breaking mechanism, so we assume it is small in the following analysis. Detailed calculations show that the contributions of f_B and f_{BB} to the most sensitive $pp \rightarrow W^+W^+jj \rightarrow l^+\nu l^+\nu jj$ channel are small even if they are of the same order of magnitude as the anomalous coupling constants f_W and f_{WW} . Hence, we shall ignore their contributions in the following analysis, and discuss only the sensitivity of the VV scatterings to the measurement of f_W and f_{WW} .

In the case that f_W dominates, the obtained numbers of events at the LHC with an integrated luminosity of 300 fb^{-1} , for various values of m_H and f_W/Λ^2 , are listed in Table IX-A and Tables X–XII. From these Tables, we see that the most sensitive channel is still $pp \rightarrow W^+W^+jj \rightarrow l^+\nu l^+\nu jj$, as listed in Table IX-A. All other channels are less interesting. Similar to the numbers in Table III, the number of the SM events (for $f_W/\Lambda^2 = 0$) is taken as the intrinsic electroweak backgrounds, i.e., $N_B = N(f_W = 0)$. The number of the signal events (for $f_W/\Lambda^2 \neq 0$) is then defined as $N_S = N(f_W \neq 0) - N_B$. We also list the values of the deviation of the signal from the total statistical fluctuation, $N_S/\sqrt{N_S + N_B}$, in the parentheses in Table IX-A. If no anomalous coupling effect is found via this process, we can set the following bounds on f_W/Λ^2 (in units of TeV^{-2}):

$$\begin{aligned} 1\sigma : & \quad -1.0 < f_W/\Lambda^2 < 0.85, \\ 2\sigma : & \quad -1.4 < f_W/\Lambda^2 \leq 1.2, \end{aligned} \quad (29)$$

for $115 \text{ GeV} \lesssim m_H \lesssim 300 \text{ GeV}$.

In the case that f_{WW} dominates, the numbers of events are listed in Table IX-B, and the corresponding bounds are (in units of TeV^{-2}) as follows:

$$\begin{aligned} 1\sigma : & \quad -1.6 \leq f_{WW}/\Lambda^2 < 1.6, \\ 2\sigma : & \quad -2.2 \leq f_{WW}/\Lambda^2 < 2.2, \end{aligned} \quad (30)$$

which are somewhat weaker than those in Eq. (29).

To see the effect of interference, we take a special case as an example, in which $f_W = -f_{WW} \equiv f$, i.e., $g_{HVV}^{(1)}$ and $g_{HVV}^{(2)}$ in Eq. (22) are of the same sign. Then we obtain the following bounds (in units of TeV^{-2}):

$$\begin{aligned} 1\sigma : & \quad -0.6 \leq f/\Lambda^2 \leq 0.5, \\ 2\sigma : & \quad -0.9 \leq f/\Lambda^2 \leq 0.75. \end{aligned} \quad (31)$$

In this case, the interference enhances the sensitivity. Of course, if $f_W = f_{WW} = f$, the sensitivity will be reduced.

From the bounds in Eqs. (29)–(30), together with the relations in Eq. (22), we obtain the corresponding bounds on $g_{HVV}^{(i)}$, $i = 1, 2$ (in units of TeV^{-1}):

$$\begin{aligned} 1\sigma : & \\ & -0.026 < g_{HWW}^{(1)} < 0.022, \\ & -0.026 < g_{HZZ}^{(1)} < 0.022, \\ & -0.014 < g_{HZZ\gamma}^{(1)} < 0.012, \\ & -0.083 \leq g_{HWW}^{(2)} < 0.083, \\ & -0.032 \leq g_{HZZ}^{(2)} < 0.032, \\ & -0.018 \leq g_{HZZ\gamma}^{(2)} < 0.018, \\ 2\sigma : & \\ & -0.036 < g_{HWW}^{(1)} \leq 0.031, \\ & -0.036 < g_{HZZ}^{(1)} \leq 0.031, \\ & -0.020 < g_{HZZ\gamma}^{(1)} \leq 0.017, \\ & -0.11 \leq g_{HWW}^{(2)} < 0.11, \\ & -0.044 \leq g_{HZZ}^{(2)} < 0.044, \\ & -0.024 \leq g_{HZZ\gamma}^{(2)} < 0.024. \end{aligned} \quad (32)$$

These bounds are to be compared with the 1σ bound on $g_{HWW}^{(2)}$ obtained from studying the on-shell Higgs boson production via weak boson fusion at the LHC, as given recently in Ref. [8]. In Ref. [8], $g_{HWW}^{(2)}$ is parameterized as $g_{HWW}^{(2)} = 1/\Lambda_5 = g^2 v/\Lambda_6^2$, and the obtained 1σ bound on Λ_6 for an integrated luminosity of 100 fb^{-1} is about $\Lambda_6 \gtrsim 1 \text{ TeV}$, which corresponds to $g_{HWW}^{(2)} = 1/\Lambda_5 \leq 0.1 \text{ TeV}^{-1}$. We see that the 1σ bounds listed in Eq. (32) are all stronger than this bound. For an integrated luminosity of 300 fb^{-1} , the bound $g_{HWW}^{(2)} = 1/\Lambda_5 \leq 0.1 \text{ TeV}^{-1}$ given in Ref. [8] corresponds roughly to a 1.7σ level of accuracy. Comparing it with the results in Eq. (32), we conclude that our 2σ bound on $g_{HWW}^{(2)}$ is at about the same level of accuracy, while our 2σ bounds on the other five $g_{HVV}^{(i)}$ ($i = 1, 2$) are all stronger than those given in Ref. [8].

It has been shown in Ref. [3] that the anomalous HZZ coupling constants $g_{HZZ}^{(1)}$ and $g_{HZZ}^{(2)}$ can be tested rather sensitively at the LC via the Higgs-strahlung process $e^+e^- \rightarrow Z^* \rightarrow Z+H$ with $Z \rightarrow ff$. In Ref. [3], $g_{HZZ}^{(1)}$ and $g_{HZZ}^{(2)}$ are parameterized as $g_{HZZ}^{(1)} = \frac{gZ}{m_Z}c_V$ and $g_{HZZ}^{(2)} = \frac{gZ}{m_Z}b_Z$, respectively. The obtained limits on the coefficients c_V and b_Z are $c_V \sim b_Z \sim O(10^{-3})$ [3] which correspond to the limits $g_{HZZ}^{(1)} \sim g_{HZZ}^{(2)} \sim$

$O(10^{-3} - 10^{-2}) \text{ TeV}^{-1}$. Although the LHC W^+W^+ scattering bounds shown in Eq. (32) are weaker than these LC bounds, W^+W^+ scattering at the LHC can provide the bounds on $g_{HWW}^{(i)}$, $i = 1, 2$. So that the two experiments are complementary to each other.

To verify that our calculation does give the correct asymptotic behavior as that given in Ref. [49], and to see the difference between the complete tree level result and the EWA result (with only the $V_L V_L \rightarrow V_L V_L$ contribution included), we plot in Fig. 5 the M_{WW} distributions in the W^+W^+ channel with $f_W/\Lambda^2 = 5 \text{ TeV}^{-2}$ from the complete tree level calculation (solid curve), the EWA calculation with the exact $W_L^+ W_L^+ \rightarrow W_L^+ W_L^+$ amplitude (dashed curve), and the result from the EWA calculation with the asymptotic formula [49] for the $W_L^+ W_L^+ \rightarrow W_L^+ W_L^+$ scattering amplitude³ (dotted curve). We see that the three curves coincide at high energies which indicates that the asymptotic behavior of the complete tree level result obtained numerically is correct. The dashed curve is significantly below the solid curve at lower energies, which shows that the signal from the transverse component contributions taken into account in the complete tree level calculation is very important. The dotted curve is much lower than the dashed curve at low energies even they are all from the EWA approach with only the longitudinal component contributions taken into account. This is because that there are contributions of energy-independent terms contained in the dashed curve which are not included in the dotted curve, and the energy-independent terms cause the dashed curve to peak significantly in the low energy region due to the larger parton luminosities in the smaller M_{WW} region. To check the correctness of this explanation, we have calculated not only the M_{WW} distribution with a constant amplitude which shows the above-mentioned peak, but also the M_{WW} distributions for the two EWA curves with a very large f_W/Λ^2 , say $f_W/\Lambda^2 = 100 \text{ TeV}^{-2}$, with which the energy-independent terms are unimportant. Indeed, the two obtained curves in this case almost completely coincide, and the peak is shifted significantly to the high energy region. Finally, we note that for the values of the anomalous couplings relevant to the bounds given in Eqs. (29) and (30), the unitarity condition is well respected, so that our full $2 \rightarrow 4$ calculation is justified. Furthermore, since in our full $2 \rightarrow 4$ calculation, we keep track on the polarization states of the final state V bosons, we can also predict the kinematical distribu-

³It only contains terms proportional to E^4 or E^2 . The E^0 contribution is not included.

tions of the final state leptons. As an example, Fig. 6 shows the distribution of the invariant mass of the dileptons from the decay of the final state W^+ bosons produced via $pp \rightarrow W^+W^+jj$ for various scenarios of the anomalous couplings. It indicates that examining in detail various kinematical distributions might help to distinguish various scenarios of new physics effect.

VII. CONCLUSIONS

We have examined the possibility of testing the anomalous HVV couplings of a light Higgs boson with mass $115 \text{ GeV} \leq m_H \leq 300 \text{ GeV}$ at the LHC via various channels of VV scatterings. This type of tests are of special interest if the anomalous HVV couplings differ from that of the SM by a significant amount so that the direct detection of the Higgs resonance is difficult. The study includes two types of anomalous HVV couplings, namely the anomalous HVV couplings from the nonlinear dimension-3 operator [13] and anomalous HVV couplings from the linearly realized dimension-6 operators [14,15]. The gold-plated pure leptonic modes are chosen for detecting the final state weak bosons. To reduce various kinds of backgrounds, we impose the kinematical cuts suggested in Ref. [17]⁴. The calculations are carried out numerically for the full cross sections of $pp \rightarrow VVjj$ including both the signals and the backgrounds under the kinematical cuts, and we take into account only the statistical uncertainties in this calculation. The results show that, with a sufficiently high integrated luminosity, such as 300 fb^{-1} , the tests of the anomalous HVV couplings can be rather sensitive. We note that to further discriminate the effect of the anomalous HVV coupling from that of a strongly interacting EWSB sector with no light resonance will eventually demand a multi-channel analysis at the LHC by searching for the light Higgs resonance through all possible on-shell production channels including gluon-gluon fusion. Once the light Higgs resonance is confirmed, VV scatterings, especially the W^+W^+ channel, can provide rather sensitive tests of various anomalous HVV couplings for probing the EWSB mechanism.

In the nonlinearly realized Higgs sector [13], the leading anomalous HVV coupling (κ) comes from the dimension-3 operator $\frac{1}{2}\kappa v H D_\mu \Sigma^\dagger D^\mu \Sigma$. The difference

⁴Although it is possible to refine the kinematic cuts to further enhance the ratio of signal to background rates, for simplicity, we applied exactly the same kinematic cuts as those proposed in Ref. [17] in this study.

$\Delta\kappa \equiv \kappa - 1$ represents the deviation from the SM value $\kappa = 1$. Our calculation shows that the most sensitive channel for testing this anomalous coupling is $pp \rightarrow W^+W^+jj \rightarrow \ell^+\nu\ell^+\nu jj$. We see from Table III that the LHC can constrain $\Delta\kappa$ to the range $-0.3 \leq \Delta\kappa \leq 0.2$ in that case that no anomalous coupling effect is detected in the channel $pp \rightarrow \ell^+\nu\ell^+\nu jj$. For comparison, several possible tests of $\Delta\kappa$ in the high energy collider experiments are also discussed in Sec. III. A summary of all the constraints considered in Sec. III is listed in Table XIII.

In the linearly realized Higgs sector [15], the leading anomalous HVV couplings arise from a set of dimension-6 operators, $\frac{f_W}{\Lambda^2}\mathcal{O}_W$, $\frac{f_{WW}}{\Lambda^2}\mathcal{O}_{WW}$, $\frac{f_B}{\Lambda^2}\mathcal{O}_B$, and $\frac{f_{BB}}{\Lambda^2}\mathcal{O}_{BB}$, as shown in Eq. (18). The anomalous HWW and HZZ couplings are expressed in Eq. (21) in terms of the anomalous coupling constants $g_{HWW}^{(1)}$, $g_{HWW}^{(2)}$, $g_{HZZ}^{(1)}$ and $g_{HZZ}^{(2)}$ which are connected to the above anomalous coupling constants f_W , f_{WW} , f_B , and f_{BB} via Eq. (22). These anomalous coupling constants are constrained by the precision electroweak data, the triple gauge coupling data, and the requirement of the unitarity of the S -matrix. Such constraints on the coupling constants f_n are given in Eqs. (23)–(27). The corresponding constraints on $g_{HWW}^{(1)}$, $g_{HWW}^{(2)}$, $g_{HZZ}^{(1)}$, and $g_{HZZ}^{(2)}$ are shown in Eq. (28) which restricts these anomalous couplings to be of $O(10^{-1}) - O(1)$. Our calculation shows that the anomalous HWW couplings can be sensitively tested via $pp \rightarrow W^+W^+jj \rightarrow \ell^+\nu\ell^+\nu jj$. Since there are several anomalous couplings from the dim-6 operators contributing to the VV scatterings, the analysis of the LHC sensitivity is more complicated than in the non-linearly realized case. If the anomalous couplings are of the same order of magnitude, the interferences depending on their relative signs could be significant. In this study, we made a single parameter analysis, i.e., assuming only one of the anomalous coupling constants is dominant at a time. Detailed calculations showed that the contributions of f_B and f_{BB} to the most sensitive $pp \rightarrow W^+W^+jj \rightarrow \ell^+\nu\ell^+\nu jj$ channel are very small even if they are of the same order of magnitude as other anomalous coupling constants. So, f_B and f_{BB} are not particularly useful in our analysis. We then analyzed the two parameters f_W and f_{WW} , separately. The 1σ and 2σ bounds on these two anomalous couplings via the most sensitive channel $pp \rightarrow W^+W^+jj \rightarrow \ell^+\nu\ell^+\nu jj$ are listed in Eqs. (29) and (30), and the corresponding bounds on the anomalous couplings $g_{HVV}^{(i)}$, $i = 1, 2$ are given in Eq. (32), i.e., the 1σ bounds are of $O(10^{-2})$, and the 2σ bounds are of $O(10^{-2} - 10^{-1})$. These bounds are stronger than that obtained from studying the on-shell Higgs boson production via weak boson fusion given in Ref. [8].

They are also complementary to the bounds on $g_{HZZ}^{(1)}$ and $g_{HZZ}^{(2)}$ at the Linear Collider (LC), as given in Ref. [3]. A summary of all the constraints considered in Sec. IV is displayed in Table XIV.

In summary, we find that *VV scatterings are not only important for probing the strongly interacting electroweak symmetry breaking mechanism when there is no light Higgs boson, but also valuable for sensitively testing of the anomalous HVV couplings (especially anomalous HWW coupling) at the LHC when there is a light Higgs boson in the mass range of 115–300 GeV*. This further supports the “no-lose” theorem [11] for the LHC to decisively probe the electroweak symmetry breaking mechanism.

Acknowledgements We would like to thank Jens Erler and Peter B. Renton for discussing the electroweak precision data, Tao Han for interesting discussions and for providing related calculation codes; and Dieter Zeppenfeld for discussing the weak boson physics. BZ and YPK are supported by the National Natural Science Foundation of China (under Grant 90103008) and Foundation of Fundamental Research of Tsinghua University; HJH and CPY are supported by the Department of Energy of USA under Grant DEFG0393ER40757, and the National Science Foundation of USA under Grant PHY-0100677, respectively.

-
- [1] R. Dashen and H. Neuberger, Phys. Rev. Lett. **50**, 1897 (1993); J. Kuti, L. Lin, and Y. Shen, *ibid.* **61**, 678 (1998); M. Lüscher and P. Weisz, Nucl. Phys. **B 318**, 705 (1989).
 - [2] L. Susskind, Phys. Rev. D **20**, 2619 (1979); G. 'tHooft, in Proceedings of *Recent Development in Gauge Theories*, New York, U.S.A., 1979.
 - [3] E.g. V. Barger, K. Cheung, A. Djouadi, B.A. Kniel, and P. M. Zerwas, Phys. Rev. D **49**, 79 (1994); M. Kramer, J. Kuhn, M. L. Stong and P. M. Zerwas, Z. Phys. C **64**, 21 (1994); K. Hagiwara and M. Stong, Z. Phys. C **62**, 99 (1994); J.F. Gunion, T. Han, and R. Sobey, Phys. Lett. B **429**, 79 (1995); K. Hagiwara, S. Ishihara, J. Kamoshita, and B.A. Kniel, Eur. Phys. J. **14**, 457 (2000).
 - [4] V. Barger, T. Han, P. Langacker, B. McElrath, and P.M. Zerwas, hep-ph/0301097.
 - [5] R.D. Heuer, D.J. Miller, F. Richard, and P.M. Zerwas (*eds.*), TESLA: Technical Design Report (Part 3), DESY 010-011, hep-ph/0106315.
 - [6] O. J. P. Éboli, M. C. Gonzalez-Garcia, S. M. Lietti, and S. F. Novaes, Phys. Lett. B **478**, 199 (2000).

- [7] F. de Campos, M. C. Gonzalez-Garcia, S. M. Lietti, S. F. Novaes, and R. Rosenfeld, Phys. Lett. B **435**, 407 (1998).
- [8] D. Zeppenfeld, hep-ph/0203123, Snowmass contribution; T. Plehn, D. Rainwater, D. Zeppenfeld, Phys. Rev. Lett. **88**, 051801 (2002).
- [9] H.-J. He, Y.-P. Kuang, C.-P. Yuan, B. Zhang, Phys. Lett. B **554**, 64 (2003) [hep-ph/0211229].
- [10] R. S. Chivukula, M. J. Dugan and M. Golden, Phys. Lett.B **336**, 62 (1994).
- [11] M. S. Chanowitz and M. K. Gaillard, Nucl. Phys. B**261** (1985) 379; Michael S. Chanowitz, Zuoz 1998, *Hidden Symmetries and Higgs Phenomena*, p.81 [hep-ph/9812215] and references therein.
- [12] H.-J. He, Y.-P. Kuang and C.-P. Yuan, Phys. Rev. D **55**, 3038 (1997); Phys. Lett.B **382**, 149 (1996).
- [13] R. Sekhar Chivukula and V. Koulovassilopoulos, Phys. Lett. B**309**, 371 (1993).
- [14] K. Hagiwara, S. Ishihara, R. Szalapski, and D. Zeppenfeld, Phys. Rev. D **48**, 2182 (1993); W. Buchmüller and D. Wyler, Nucl. Phys. B**268**, 621 (1986); C. J. C. Burgess and H. J. Schnitzer, Nucl. Phys. B**228**, 454 (1983); C. N. Leung, S. T. Love and S. Rao, Z. Phys. **31**, 433 (1986); A. De Rújula, M. B. Gavela, P. Hernández and E. Massó, Nucl. Phys. B **384**, 3 (1992).
- [15] For a review, M. C. Gonzalez-Garcia, Int. J. Mod. Phys. A **14**, 3121 (1999).
- [16] J. Bagger, V. Barger, K. Cheung, J. Gunion, T. Han, G. Ladinsky, R. Rosenfeld, and C.-P. Yuan, Phys. Rev. D **49**, 1246 (1994).
- [17] J. Bagger, V. Barger, K. Cheung, J. Gunion, T. Han, G. Ladinsky, R. Rosenfeld, and C.-P. Yuan, Phys. Rev. D **52**, 3878 (1995);
- [18] V. Barger, K. Cheung, T. Han, and R.J.N. Phillips, Phys. Rev. D **42**, 3052 (1990).
- [19] C.-P. Yuan “Proposals for Studying TeV $W_L W_L \rightarrow W_L W_L$ Interactions Experiments”, [hep-ph/9712513], in *Perspectives on Higgs Physics*, second edition, edited by G. L. Kane (World Scientific, Singapore).
- [20] J. Pumplin, D.R. Stump, J. Huston, H.L. Lai, P. Nadolsky, W.K. Tung, JHEP **0207**,012 (2002).
- [21] M. S. Chanowitz and M. K. Gaillard, Phys. Lett. B **142**, 85 (1984); G. L. Kane, W. W. Repko, W. R. Rolnik, Phys. Lett. B **148**,367 (1984); S. Dawson, Nucl. Phys. B **249**,427 (1985).
- [22] E. Boos, H.-J. He, W. Kilian, A. Pukhov, C.-P. Yuan, and P.M. Zerwas, Phys. Rev. D **57**, 1553 (1998); Phys. Rev. D **61**, 077901 (2000).
- [23] A. Manohar and H. Georgi, Nucl. Phys. B **234**, 189 (1984).
- [24] M.E. Peskin and T. Takeuchi, Phys. Rev. D **46**, 381 (1992).
- [25] T. Appelquist and C. Bernard, Phys. Rev. D **22**, 200 (1980); A. C. Longhitano, Nucl. Phys. B **188**, 118 (1981).
- [26] E.g., S. Dawson and G. Valencia, Nucl. Phys. B **439**, 3 (1995).
- [27] H. Georgi, Ann. Rev. Nucl. & Part. Sci. **43**, 209 (1994), and references therein.
- [28] Particle Data Group (K. Hagiwara *et al.*), Phys. Rev. D **66**, 010001 (2002).
- [29] B. A. Dobrescu and C. T. Hill, Phys. Rev. Lett. **81**, 2634 (1998); R. S. Chivukula, B. A. Dobrescu, H. Georgi, and C. T. Hill, Phys. Rev. D **59**, 075003 (1999); H.-J. He, C. T. Hill, and T. Tait, Phys. Rev. D **65**, 055006 (2002); H.-J. He, T. Tait, and C.-P. Yuan, Phys. Rev. D **62**, 011702 (2000) (R).
- [30] J. Bagger, A. F. Falk and M. Swartz, Phys. Rev. Lett. **84**, 1385 (2000); R. S. Chivukula, C. Hölbling and N. Evans, Phys. Rev. Lett. **85**, 511 (2000); C. Kolda and H. Murayama, JHEP **0007**, 035 (2000); M. E. Peskin and J. D. Wells, Phys. Rev. D **64**, 093003 (2001).
- [31] H.-J. He, N. Polonsky and S. Su, Phys. Rev. D **64**, 053004 (2001) [hep-ph/0102144].
- [32] R. Sekhar Chivukula and C. Hölbling, eConf C010630: P105 (2001) [hep-ph/0110214].
- [33] M. S. Chanowitz, Phys. Rev. D **66**, 073002 (2002) [hep-ph/0207123].
- [34] E.g., G. A. Miller and A. W. Thomas, hep-ex/0204007; S. Davidson, To appear in Proc. First International School on Neutrino Factory: NuFact02 Summer Institute, Abington, Oxford, England, 24-29 June, 2002 [hep-ph/0209316].
- [35] J. Erler, private communications, hep-ph/0005084 and review at <http://pdg.lbl.gov>; P. Langacker, J.Phys. G **29**, 1 (2003) [hep-ph/0211065].
- [36] M. W. Grünewald, talk at ICHEP, Amsterdam, July 24-31, 2002 [hep-ex/0210003], and LEP Electroweak Working Group, <http://www.cern.ch/LEPEWWG>; see also, P. B. Renton, Rept. Prog. Phys. **65**, 1271 (2002) [hep-ph/0206231].
- [37] For an updated comprehensive review, C. T. Hill and E. H. Simmons, hep-ph/0203079.
- [38] E. Malkawi and C.-P. Yuan, Phys. Rev. D**52** (1995) 472; F. Larios, M.A. Perez and C.-P. Yuan, Phys. Lett. B**457** (1999) 334.
- [39] H.-J. He, Y.-P. Kuang and C.-P. Yuan, Phys. Rev. D **55**, 3038 (1997) [hep-ph/9611316]; Phys. Lett. B **382**, 149 (1996) [hep-ph/9604309]; CCAST-WL Workshop Series **72**, 119 (1996) [hep-ph/9704276].
- [40] ALEPH, DELPHI, L3 and OPAL (The LEP working group for Higgs searches), talk presented at 2001 International Symposium on Lepton and Photon Interactions at High Energies, Rome, 2001, hep-ex/0107029; U. Schwickerath, hep-ph/0205126.
- [41] P. Agrawal, Mod. Phys. Lett. A **16**, 897 (2001) [hep-ph/0011347].
- [42] V. Drollinger and A. Sopczak, Eur. Phys. J. direct C **3**, N1 (2001) [hep-ph/0102342].
- [43] F. Gianotti, *et al.*, CERN-TH/2002-078, hep-ph/0204087.
- [44] D. Zeppenfeld, eConf C010630: P123 (2001) [hep-ph/0203123].
- [45] K. Hagiwara, S. Ishihara, R. Szalapski and D. Zeppenfeld, Phys. Lett. B **283**, 353 (1992); Phys. Rev. D **48**, 2182 (1993).
- [46] S. Alam, S. Dawson, R. Szalapski, Phys. Rev. D **57**, 1577 (1998); K. Hagiwara, S. Matsumoto R. Szalapski,

- Phys. Lett. B **357**, 411 (1995).
- [47] B. Abbott *et al.*, D0 Collaboration, Phys. Rev. D **58**, 031102 (1998).
- [48] ALEPH Collaboration, R. Barate *et al.*, Phys. Lett. B **422**, 369 (1998); DELPHI Collaboration, P. Abreu *et al.*, Phys. Lett. B **423**, 194 (1998); L3 Collaboration, M. Acciari *et al.*, Phys. Lett. B **413**, 176 (1998); OPAL Collaboration, K. Ackerstaff *et al.*, Eur. Phys. J. **C2**, 597 (1998).
- [49] G.J. Gounaris, J. Layssac, and F.M. Renard, Phys. Lett. B **332**, 146 (1994); G.J. Gounaris, J. Layssac, J.E. Pascalis, and F.M. Renard, Z. Phys. C **66**, 619 (1995).

TABLES

Table I. The 95% C.L. limits on $\Delta\kappa$ imposed by Z -pole and low energy precision electroweak data, for a few typical values of new physics scale Λ and Higgs boson mass m_H .

| m_H (GeV) | Λ (TeV) | | |
|-------------|--------------------------------------|--------------------------------------|--------------------------------------|
| | 1 | 10 | 100 |
| 115 | $-0.15 \leq \Delta\kappa \leq 0.23$ | $-0.069 \leq \Delta\kappa \leq 0.12$ | $-0.045 \leq \Delta\kappa \leq 0.08$ |
| 300 | $-0.074 \leq \Delta\kappa \leq 0.60$ | $0.027 \leq \Delta\kappa \leq 0.24$ | $0.016 \leq \Delta\kappa \leq 0.15$ |
| 800 | (excluded) | $0.20 \leq \Delta\kappa \leq 0.45$ | $0.11 \leq \Delta\kappa \leq 0.26$ |

Table II. Cross section $\sigma_{\lambda_1\lambda_2}$ (in units of fb) of $pp \rightarrow W_{\lambda_1}^+ W_{\lambda_2}^+ jj$ at the LHC for various values of $\Delta\kappa$ with $m_H = 115$ GeV. W_{λ}^+ denotes a polarized W boson with the polarization index $\lambda = T$ or L .

| $\Delta\kappa$ | σ_{all} | σ_{LL} | σ_{LT} | σ_{TT} |
|----------------|-----------------------|---------------|---------------|---------------|
| 0.0 | 1.1 | 0.02 | 0.2 | 0.8 |
| 0.4 | 4.1 | 3.0 | 0.3 | 0.8 |

Table III. Number of events at the LHC, with an integrated luminosity of 300 fb^{-1} , for $pp \rightarrow W^{\pm} W^{\pm} jj \rightarrow l^{\pm} \nu(\bar{\nu}) l^{\pm} \nu(\bar{\nu}) jj$ ($l^{\pm} = e^{\pm}$ or μ^{\pm}) with various values of m_H and $\Delta\kappa$. ($\Delta\kappa = 0$ corresponds to the SM.) The values of $N_S/\sqrt{N_S + N_B}$ are also shown in the parentheses.

| $pp \rightarrow W^+ W^+ jj \rightarrow l^+ \nu l^+ \nu jj$ | | | | | | | | | | | |
|--|----------------|----------|----------|-----|----------|----------|----------|----------|----------|------------|--|
| m_H (GeV) | $\Delta\kappa$ | | | | | | | | | | |
| | -1.0 | -0.6 | -0.3 | 0.0 | 0.2 | 0.3 | 0.4 | 0.5 | 0.6 | 0.7 | |
| 115 | 62 (6.0) | 48 (4.8) | 27 (2.3) | 15 | 24 (1.8) | 37 (3.6) | 58 (5.6) | — | — | — | |
| 130 | 62 (6.0) | 48 (4.8) | 27 (2.3) | 15 | 24 (1.8) | 37 (3.6) | 57 (5.5) | — | — | — | |
| 200 | 62 (6.0) | 48 (4.8) | 28 (2.5) | 15 | 22 (1.5) | 33 (3.1) | 52 (5.1) | 78 (7.1) | — | — | |
| 300 | 61 (5.9) | 49 (4.9) | 30 (2.7) | 16 | 20 (1.1) | 29 (2.6) | 43 (4.3) | 65 (6.2) | 95 (8.2) | 136 (10.4) | |

| $pp \rightarrow W^- W^- jj \rightarrow l^- \bar{\nu} l^- \bar{\nu} jj$ | | | | | | | | | | | |
|--|----------------|------|------|-----|-----|-----|-----|-----|-----|-----|--|
| m_H (GeV) | $\Delta\kappa$ | | | | | | | | | | |
| | -1.0 | -0.6 | -0.3 | 0.0 | 0.2 | 0.3 | 0.4 | 0.5 | 0.6 | 0.7 | |
| 115 | 13 | 10 | 6 | 3 | 4 | 6 | 9 | — | — | — | |
| 130 | 13 | 10 | 6 | 3 | 4 | 6 | 9 | — | — | — | |
| 200 | 13 | 10 | 6 | 3 | 4 | 6 | 8 | 11 | — | — | |
| 300 | 13 | 10 | 6 | 4 | 4 | 5 | 7 | 10 | 14 | 19 | |

Table IV. Number of events at the LHC, with an integrated luminosity of 300 fb^{-1} , for $pp \rightarrow W^+W^-jj \rightarrow l^+\nu l^-\nu jj$ ($l^\pm = e^\pm$ or μ^\pm) with various values of m_H and $\Delta\kappa$. ($\Delta\kappa = 0$ corresponds to the SM.)

| $m_H(\text{GeV})$ | $\Delta\kappa$ | | | | | | | | | |
|-------------------|----------------|------|------|-----|-----|-----|-----|-----|-----|-----|
| | -1.0 | -0.6 | -0.3 | 0.0 | 0.2 | 0.3 | 0.4 | 0.5 | 0.6 | 0.7 |
| 115 | 19 | 14 | 8 | 4 | 7 | 11 | 17 | – | – | – |
| 130 | 19 | 14 | 8 | 4 | 7 | 11 | 17 | – | – | – |
| 200 | 19 | 14 | 8 | 4 | 8 | 12 | 19 | 29 | – | – |
| 300 | 19 | 14 | 7 | 4 | 9 | 14 | 23 | 34 | 48 | 69 |

Table V. Number of events at the LHC, with an integrated luminosity of 300 fb^{-1} , for $pp \rightarrow ZW^\pm jj \rightarrow l^+l^-l^\pm\nu(\bar{\nu})jj$ ($l^\pm = e^\pm$ or μ^\pm) with various values of m_H (in GeV) and $\Delta\kappa$. ($\Delta\kappa = 0$ corresponds to the SM.)

| $pp \rightarrow ZW^+jj \rightarrow l^+l^-l^+\nu jj$ | | | | | | | | | | | |
|---|----------------|------|------|-----|-----|-----|-----|-----|-----|-----|--|
| $m_H(\text{GeV})$ | $\Delta\kappa$ | | | | | | | | | | |
| | -1.0 | -0.6 | -0.3 | 0.0 | 0.2 | 0.3 | 0.4 | 0.5 | 0.6 | 0.7 | |
| 115 | 9 | 7 | 4 | 2 | 3 | 5 | 7 | – | – | – | |
| 130 | 9 | 7 | 4 | 2 | 3 | 5 | 7 | – | – | – | |
| 200 | 9 | 7 | 4 | 2 | 3 | 4 | 6 | 10 | – | – | |
| 300 | 9 | 7 | 4 | 2 | 3 | 4 | 5 | 9 | 12 | 16 | |

| $pp \rightarrow ZW^-jj \rightarrow l^+l^-l^-\bar{\nu} jj$ | | | | | | | | | | | |
|---|----------------|------|------|-----|-----|-----|-----|-----|-----|-----|--|
| $m_H(\text{GeV})$ | $\Delta\kappa$ | | | | | | | | | | |
| | -1.0 | -0.6 | -0.3 | 1.0 | 0.2 | 0.3 | 0.4 | 0.5 | 0.6 | 0.7 | |
| 115 | 4 | 3 | 2 | 1 | 1 | 2 | 3 | – | – | – | |
| 130 | 4 | 3 | 2 | 1 | 1 | 2 | 3 | – | – | – | |
| 200 | 4 | 3 | 2 | 1 | 1 | 2 | 3 | 4 | – | – | |
| 300 | 4 | 3 | 2 | 1 | 1 | 2 | 2 | 4 | 5 | 7 | |

Table VI. Number of events at the LHC, with an integrated luminosity of 300 fb^{-1} for $pp \rightarrow ZZjj \rightarrow l^+l^-l^+l^-(\nu\bar{\nu})jj$ ($l^\pm = e^\pm$ or μ^\pm) with various values of m_H (in GeV) and $\Delta\kappa$. ($\Delta\kappa = 0$ corresponds to the SM.)

| $pp \rightarrow ZZjj \rightarrow l^+l^-l^+l^-jj$ | | | | | | | | | | |
|--|------|------|------|-----|----------------|-----|-----|-----|-----|-----|
| $m_H(\text{GeV})$ | -1.0 | -0.6 | -0.3 | 0.0 | $\Delta\kappa$ | 0.3 | 0.4 | 0.5 | 0.6 | 0.7 |
| 115 | 9 | 8 | 5 | 4 | 5 | 6 | 8 | — | — | — |
| 130 | 9 | 8 | 5 | 4 | 5 | 6 | 8 | — | — | — |
| 200 | 9 | 8 | 5 | 4 | 5 | 7 | 9 | 13 | — | — |
| 300 | 9 | 7 | 5 | 4 | 6 | 9 | 12 | 17 | 24 | 32 |

| $pp \rightarrow ZZjj \rightarrow l^+l^-\nu\bar{\nu}jj$ | | | | | | | | | | |
|--|------|------|------|-----|----------------|-----|-----|-----|-----|-----|
| $m_H(\text{GeV})$ | -1.0 | -0.6 | -0.3 | 0.0 | $\Delta\kappa$ | 0.3 | 0.4 | 0.5 | 0.6 | 0.7 |
| 115 | 5 | 4 | 2 | 0 | 1 | 3 | 5 | — | — | — |
| 130 | 5 | 4 | 2 | 0 | 1 | 3 | 5 | — | — | — |
| 200 | 5 | 4 | 2 | 0 | 1 | 3 | 5 | 8 | — | — |
| 300 | 5 | 4 | 2 | 0 | 1 | 3 | 6 | 9 | 14 | 20 |

Table VII. Decay branching ratio $B(H \rightarrow \gamma\gamma)$, in the unit of 10^{-3} , as a function of $\Delta\kappa$ for various m_H .

| $m_H(\text{GeV})$ | -0.4 | -0.3 | -0.2 | -0.1 | -0.05 | $\Delta\kappa$ | 0.0 | 0.05 | 0.1 | 0.2 | 0.3 | 0.4 |
|-------------------|------|------|------|------|-------|----------------|-----|------|-----|-----|-----|-----|
| 110 | 2.8 | 2.4 | 2.2 | 2.0 | 2.0 | 1.9 | 1.9 | 1.8 | 1.8 | 1.7 | 1.7 | 1.7 |
| 120 | 4.3 | 3.2 | 2.7 | 2.4 | 2.3 | 2.2 | 2.1 | 2.1 | 1.9 | 1.8 | 1.7 | 1.7 |
| 130 | 6.7 | 4.4 | 3.2 | 2.6 | 2.4 | 2.3 | 2.1 | 2.0 | 1.8 | 1.6 | 1.5 | 1.5 |

Table VIII. Decay branching ratio $B(\kappa) \equiv B(H \rightarrow WW^*)$ as a function of $|\kappa|$ for various m_H .

| $m_H(\text{GeV})$ | 0.6 | 0.7 | 0.8 | 0.9 | 0.95 | $ \kappa $ | 1.0 | 1.05 | 1.1 | 1.2 | 1.3 | 1.4 |
|-------------------|-------|-------|-------|------|-------|------------|-------|-------|-------|-------|-------|-------|
| 110 | 0.013 | 0.018 | 0.024 | 0.03 | 0.033 | 0.037 | 0.040 | 0.044 | 0.052 | 0.061 | 0.069 | 0.069 |
| 120 | 0.048 | 0.064 | 0.082 | 0.10 | 0.11 | 0.12 | 0.13 | 0.14 | 0.17 | 0.19 | 0.21 | 0.21 |
| 130 | 0.12 | 0.16 | 0.20 | 0.24 | 0.26 | 0.28 | 0.30 | 0.32 | 0.35 | 0.39 | 0.42 | 0.42 |
| 150 | 0.48 | 0.55 | 0.60 | 0.65 | 0.67 | 0.68 | 0.70 | 0.71 | 0.74 | 0.76 | 0.78 | 0.78 |
| 170 | 0.95 | 0.95 | 0.96 | 0.96 | 0.96 | 0.97 | 0.97 | 0.97 | 0.97 | 0.97 | 0.97 | 0.97 |

Table IX-A. Number of events at the LHC, with an integrated luminosity of 300 fb^{-1} , for $pp \rightarrow W^\pm W^\pm \rightarrow l^\pm \nu l^\pm \nu jj$ ($l^\pm = e^\pm$ or μ^\pm) in the linearly realized effective Lagrangian with various values of m_H and f_W/Λ^2 . The values of $N_S/\sqrt{N_S + N_B}$ are also shown in the parentheses.

| $pp \rightarrow W^+ W^+ jj \rightarrow l^+ \nu l^+ \nu jj$ | | | | | | | | | | | |
|--|--------------------------------|---------|---------|---------|---------|-----|---------|---------|---------|---------|---------|
| m_H (GeV) | f_W/Λ^2 (TeV $^{-2}$) | | | | | | | | | | |
| | -4.0 | -3.0 | -2.0 | -1.4 | -1.0 | 0.0 | 0.85 | 1.2 | 2.0 | 3.0 | 4.0 |
| 115 | 117(9.4) | 72(6.7) | 38(3.7) | 26(2.2) | 20(1.1) | 15 | 20(1.1) | 25(2.0) | 42(4.2) | 78(7.1) | 129(10) |
| 130 | 118(9.5) | 72(6.7) | 38(3.7) | 26(2.2) | 20(1.1) | 15 | 20(1.1) | 25(2.0) | 42(4.2) | 78(7.1) | 130(10) |
| 200 | 119(9.5) | 73(6.8) | 38(3.7) | 26(2.2) | 20(1.1) | 15 | 20(1.1) | 25(2.0) | 42(4.2) | 79(7.2) | 132(10) |
| 300 | 121(9.6) | 75(6.9) | 39(3.8) | 27(2.3) | 21(1.3) | 16 | 21(1.3) | 26(2.2) | 43(4.3) | 80(7.3) | 134(10) |

| $pp \rightarrow W^- W^- jj \rightarrow l^- \bar{\nu} l^- \bar{\nu} jj$ | | | | | | | | | | | |
|--|--------------------------------|------|------|------|------|-----|------|-----|-----|-----|-----|
| m_H (GeV) | f_W/Λ^2 (TeV $^{-2}$) | | | | | | | | | | |
| | -4.0 | -3.0 | -2.0 | -1.4 | -1.0 | 0.0 | 0.85 | 1.2 | 2.0 | 3.0 | 4.0 |
| 115 | 23 | 14 | 7 | 5 | 4 | 3 | 4 | 5 | 8 | 15 | 25 |
| 130 | 23 | 14 | 7 | 5 | 4 | 3 | 4 | 5 | 8 | 15 | 25 |
| 200 | 23 | 14 | 7 | 5 | 4 | 3 | 4 | 5 | 8 | 15 | 26 |
| 300 | 24 | 15 | 8 | 5 | 4 | 4 | 4 | 5 | 8 | 16 | 26 |

Table IX-B. Number of events at the LHC, with an integrated luminosity 300 fb^{-1} , for $pp \rightarrow W^\pm W^\pm \rightarrow l^\pm \nu l^\pm \nu jj$ ($l^\pm = e^\pm$ or μ^\pm) in the linearly realized effective Lagrangian with various values of m_H and f_{WW}/Λ^2 . The values of $N_S/\sqrt{N_S + N_B}$ are also shown in the parentheses.

| $pp \rightarrow W^+ W^+ jj \rightarrow l^+ \nu l^+ \nu jj$ | | | | | | | | | | |
|--|-----------------------------------|---------|---------|---------|-----|---------|---------|---------|---------|--|
| m_H (GeV) | f_{WW}/Λ^2 (TeV $^{-2}$) | | | | | | | | | |
| | -4.0 | -3.0 | -2.2 | -1.6 | 0.0 | 1.6 | 2.2 | 3.0 | 4.0 | |
| 115 | 47(4.7) | 33(3.1) | 25(2.0) | 19(0.9) | 15 | 20(1.1) | 26(2.2) | 33(3.1) | 48(4.8) | |
| 130 | 48(4.8) | 33(3.1) | 25(2.0) | 19(0.9) | 15 | 20(1.1) | 26(2.2) | 34(3.1) | 49(4.9) | |
| 200 | 49(4.9) | 34(3.3) | 25(2.0) | 19(0.9) | 15 | 20(1.1) | 26(2.2) | 35(3.4) | 50(4.9) | |
| 300 | 51(5.0) | 35(3.4) | 26(2.2) | 20(1.1) | 16 | 21(1.3) | 27(2.3) | 36(3.5) | 52(5.1) | |

| $pp \rightarrow W^- W^- jj \rightarrow l^- \bar{\nu} l^- \bar{\nu} jj$ | | | | | | | | | | |
|--|-----------------------------------|------|------|------|-----|-----|-----|-----|-----|--|
| m_H (GeV) | f_{WW}/Λ^2 (TeV $^{-2}$) | | | | | | | | | |
| | -4.0 | -3.0 | -2.2 | -1.6 | 0.0 | 1.6 | 2.2 | 3.0 | 4.0 | |
| 115 | 9 | 6 | 5 | 4 | 3 | 4 | 5 | 6 | 9 | |
| 130 | 9 | 6 | 5 | 4 | 3 | 4 | 5 | 7 | 10 | |
| 200 | 10 | 7 | 5 | 4 | 3 | 4 | 5 | 7 | 10 | |
| 300 | 10 | 7 | 5 | 4 | 4 | 4 | 5 | 7 | 10 | |

Table X. Number of events at the LHC, with an integrated luminosity of 300 fb^{-1} , for $pp \rightarrow W^+ W^- jj \rightarrow l^+ \nu l^- \nu jj$ ($l^\pm = e^\pm$ or μ^\pm) in the linearly realized effective Lagrangian with various values of m_H and f_W/Λ^2 .

| m_H (GeV) | f_W/Λ^2 (TeV $^{-2}$) | | | | | | | | | |
|-------------|--------------------------------|------|------|------|-----|-----|-----|-----|-----|--|
| | -4.0 | -3.0 | -2.0 | -1.0 | 0.0 | 1.0 | 2.0 | 3.0 | 4.0 | |
| 115 | 35 | 21 | 10 | 5 | 4 | 6 | 12 | 23 | 38 | |
| 130 | 35 | 21 | 10 | 5 | 4 | 6 | 12 | 23 | 38 | |
| 200 | 36 | 21 | 10 | 5 | 4 | 6 | 12 | 23 | 39 | |
| 300 | 37 | 22 | 11 | 5 | 4 | 6 | 13 | 24 | 40 | |

Table XI. Number of events at the LHC, with an integrated luminosity 300 fb^{-1} , for $pp \rightarrow ZZjj \rightarrow l^+l^-l^+l^- (l^+l^- \nu\bar{\nu})jj$ ($l^\pm = e^\pm$ or μ^\pm) in the linearly realized effective Lagrangian with various values of m_H and f_W/Λ^2 .

| $pp \rightarrow ZZjj \rightarrow l^+l^- \nu\bar{\nu}jj$ | | | | | | | | | | |
|---|-----------------------------------|------|------|------|-----|-----|-----|-----|-----|--|
| $m_H(\text{GeV})$ | $f_W/\Lambda^2 (\text{TeV}^{-2})$ | | | | | | | | | |
| | -4.0 | -3.0 | -2.0 | -1.0 | 0.0 | 1.0 | 2.0 | 3.0 | 4.0 | |
| 115 | 10 | 6 | 2 | 1 | 0 | 1 | 3 | 6 | 11 | |
| 130 | 10 | 6 | 2 | 1 | 0 | 1 | 3 | 6 | 11 | |
| 200 | 10 | 6 | 2 | 1 | 0 | 1 | 3 | 6 | 11 | |
| 300 | 10 | 6 | 2 | 1 | 0 | 1 | 3 | 6 | 12 | |

| $pp \rightarrow ZZjj \rightarrow l^+l^-l^+l^-jj$ | | | | | | | | | | |
|--|-----------------------------------|------|------|------|-----|-----|-----|-----|-----|--|
| $m_H(\text{GeV})$ | $f_W/\Lambda^2 (\text{TeV}^{-2})$ | | | | | | | | | |
| | -4.0 | -3.0 | -2.0 | -1.0 | 0.0 | 1.0 | 2.0 | 3.0 | 4.0 | |
| 115 | 9 | 7 | 5 | 4 | 4 | 5 | 6 | 8 | 10 | |
| 130 | 9 | 7 | 5 | 4 | 4 | 5 | 6 | 8 | 10 | |
| 200 | 9 | 7 | 5 | 4 | 4 | 5 | 6 | 8 | 10 | |
| 300 | 9 | 7 | 5 | 4 | 4 | 5 | 6 | 8 | 11 | |

Table XII. Number of events at the LHC, with an integrated luminosity 300 fb^{-1} , for $pp \rightarrow ZW^\pm jj \rightarrow l^\pm \nu l^\pm jj$ ($l^\pm = e^\pm$ or μ^\pm) in the linearly realized effective Lagrangian with various values of m_H and f_W/Λ^2 .

| $pp \rightarrow ZW^+jj \rightarrow l^+l^-l^+\nu jj$ | | | | | | | | | | |
|---|-----------------------------------|------|------|------|-----|-----|-----|-----|-----|--|
| $m_H(\text{GeV})$ | $f_W/\Lambda^2 (\text{TeV}^{-2})$ | | | | | | | | | |
| | -4.0 | -3.0 | -2.0 | -1.0 | 0.0 | 1.0 | 2.0 | 3.0 | 4.0 | |
| 115 | 10 | 7 | 4 | 3 | 2 | 3 | 5 | 8 | 12 | |
| 130 | 10 | 7 | 4 | 3 | 2 | 3 | 5 | 8 | 12 | |
| 200 | 10 | 7 | 4 | 3 | 2 | 3 | 5 | 8 | 12 | |
| 300 | 10 | 7 | 4 | 3 | 2 | 3 | 5 | 8 | 12 | |

| $pp \rightarrow ZW^-jj \rightarrow l^+l^-l^-\bar{\nu}jj$ | | | | | | | | | | |
|--|-----------------------------------|------|------|------|-----|-----|-----|-----|-----|--|
| $m_H(\text{GeV})$ | $f_W/\Lambda^2 (\text{TeV}^{-2})$ | | | | | | | | | |
| | -4.0 | -3.0 | -2.0 | -1.0 | 0.0 | 1.0 | 2.0 | 3.0 | 4.0 | |
| 115 | 4 | 2 | 1 | 1 | 1 | 1 | 1 | 2 | 4 | |
| 130 | 4 | 2 | 1 | 1 | 1 | 1 | 1 | 2 | 4 | |
| 200 | 4 | 2 | 1 | 1 | 1 | 1 | 1 | 2 | 4 | |
| 300 | 4 | 2 | 1 | 1 | 1 | 1 | 1 | 2 | 4 | |

Table XIII. Summary of the 2σ constraints on the anomalous HVV coupling κ ($\equiv 1 + \Delta\kappa$) from the dimension-3 operator in the nonlinear Higgs sector studied in Sec. III.

| Types of constraints | results | Places in the text |
|--------------------------------------|---|--------------------|
| Precision EW data | regions shown in Figs. 2 and 3, Table I | Eq. (7) |
| Unitarity (at $\sqrt{s}=2$ TeV) | $0.5 < \kappa < 1.3$ | Eq. (11) |
| W^+W^+ scattering | $-0.3 < \Delta\kappa < 0.2$ | Eq. (13) |
| HV production ($m_H = 120$ GeV) | $0 \leq \kappa \leq 1.6$ | Eq. (14) |
| Higgs width ($m_H = 200 - 300$ GeV) | $0.8 \leq \kappa \leq 1.2$ | Eq. (15) |
| $B(H \rightarrow \gamma\gamma)$ | Table VII | Sec. V-C |
| Higgs resonance ($m_H = 120$ GeV) | $0.88 \leq R \leq 1.12$ [$R \equiv \kappa^2 B(\kappa)/B(\kappa = 1)$], Table VIII | Eq. (16) |
| LC (500 GeV, 1ab^{-1}) | $ \Delta\kappa \leq 0.3\%$ | Sec. V-E |

Table XIV. Summary of the 2σ constraints on the anomalous couplings f_n/Λ^2 (in units of TeV^{-2}) associated with the dimension-6 operators [cf. Eqs. (17)–(19)] and the related form factors $g_{HVV}^{(1)}$ and $g_{HVV}^{(2)}$ (in units of TeV^{-1}) [cf. Eq. (22)] in the linearly realized Higgs sector studied in Sec. IV.

| types of constraints | results | places in the text | |
|---|---|--|----------------------|
| precision EW data | 2-parameter fit at tree level: regions shown in Fig. 4, with $-0.05 < \frac{f_{\Phi,1}}{\Lambda^2} < 0.02, \quad -0.10 < \frac{f_{BW}}{\Lambda^2} < 0.05.$ | Fig. 4 | |
| | 1-parameter fit at 1-loop level: $-6 \leq \frac{f_{WWW}}{\Lambda^2} \leq 3, \quad -6 \leq \frac{f_W}{\Lambda^2} \leq 5, \quad -4.2 \leq \frac{f_B}{\Lambda^2} \leq 2.0,$ $-5.0 \leq \frac{f_{WW}}{\Lambda^2} \leq 5.6, \quad -17 \leq \frac{f_{BB}}{\Lambda^2} \leq 20.$ | Eq. (23) | |
| triple gauge coupling data | $-31 \leq \frac{(f_W + f_B)}{\Lambda^2} \leq 68 \text{ (for } f_{WWW} = 0),$ $-41 \leq \frac{f_{WWW}}{\Lambda^2} \leq 26 \text{ (for } f_W + f_B = 0).$ | Eq. (24) | |
| LEP2 Higgs searches | $-7.5 \leq \frac{f_{WW(BB)}}{\Lambda^2} \leq 18.$ | Eq. (25) | |
| unitarity requirement (at $\sqrt{s}=2$ TeV) | $ \frac{f_b}{\Lambda^2} \leq 24.5, \quad \frac{f_W}{\Lambda^2} \leq 7.8, \quad \frac{f_{WWW}}{\Lambda^2} \leq 7.5,$ $-160 \leq \frac{f_{BB}}{\Lambda^2} \leq 197, \quad \frac{f_{WW}}{\Lambda^2} \leq 39.2.$ | Eq. (27) | |
| W^+W^+ scattering | 1σ $-1.0 < \frac{f_W}{\Lambda^2} < 0.85,$ $-1.6 < \frac{f_{WW}}{\Lambda^2} < 1.6,$ | 2σ $-1.4 < \frac{f_W}{\Lambda^2} \leq 1.2.$ $-2.2 \leq \frac{f_{WW}}{\Lambda^2} < 2.2.$ | Eq. (29) Eq. (30) |
| | or | | |
| | $-0.026 < g_{HWW}^{(1)} < 0.022, \quad -0.036 < g_{HWW}^{(1)} \leq 0.031.$ $-0.026 < g_{HZZ}^{(1)} < 0.022, \quad -0.036 < g_{HZZ}^{(1)} \leq 0.031.$ $-0.014 < g_{HZZ\gamma}^{(1)} < 0.012, \quad -0.020 < g_{HZZ\gamma}^{(1)} \leq 0.017.$ $-0.083 < g_{HWW}^{(2)} < 0.083, \quad -0.11 \leq g_{HWW}^{(2)} < 0.11.$ $-0.032 < g_{HZZ}^{(2)} < 0.032, \quad -0.044 \leq g_{HZZ}^{(2)} < 0.044.$ $-0.018 < g_{HZZ\gamma}^{(2)} < 0.018, \quad -0.024 \leq g_{HZZ\gamma}^{(2)} < 0.024.$ | Eq. (31) | |
| HVV coupling at LC (500 GeV, 1ab^{-1}) | $ \frac{f_{\Phi,2}}{\Lambda^2} < 0.2$ | Sec. VI-A | |

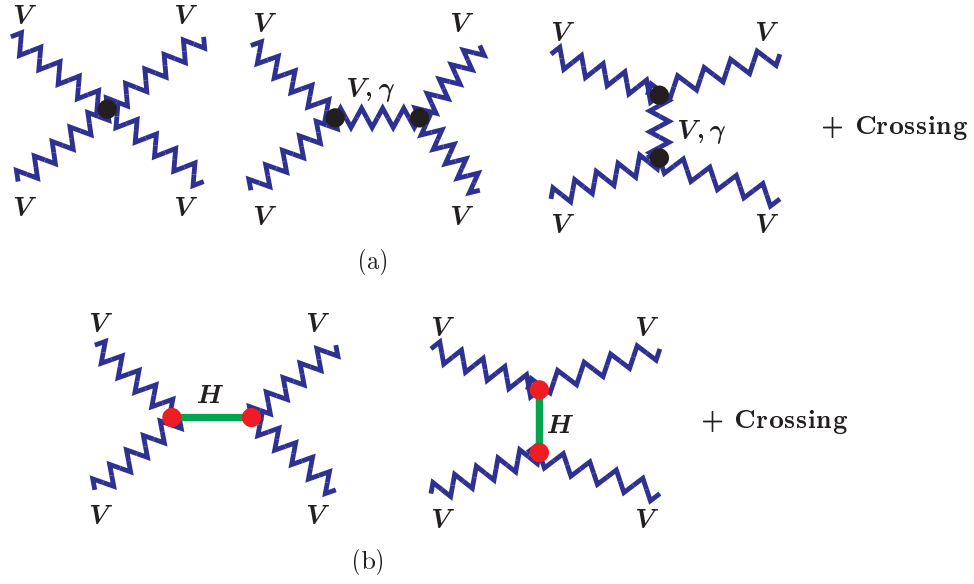


FIG. 1. Illustration of Feynman diagrams for VV scatterings in the SM: (a) diagrams contributing to $T(V, \gamma)$, (b) diagrams contributing to $T(H)$.

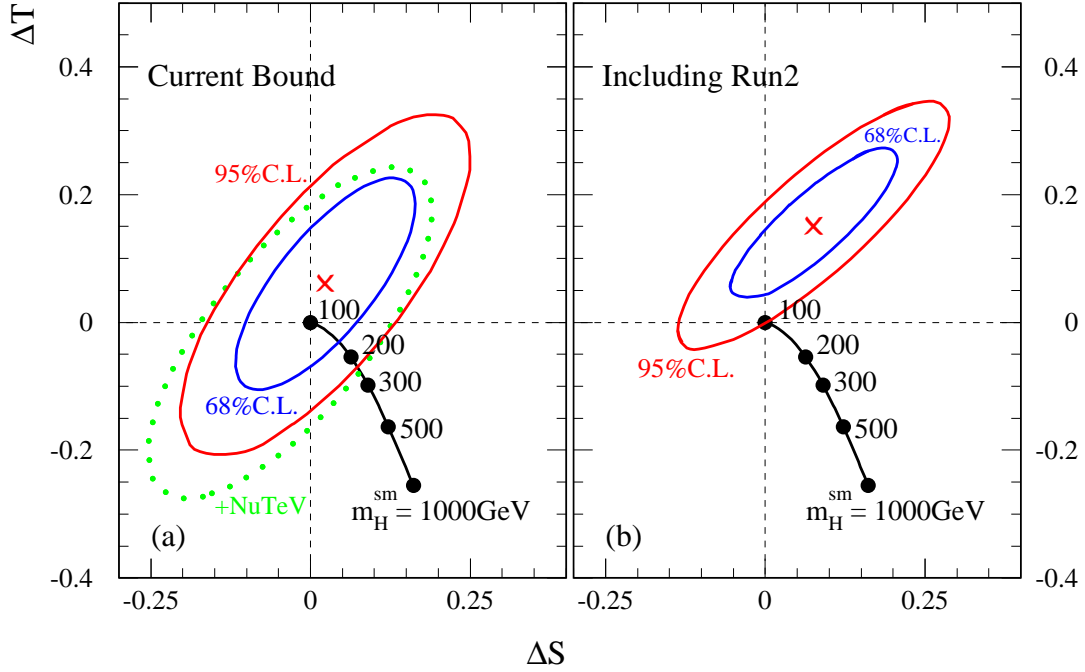


FIG. 2. $\Delta S - \Delta T$ contours (a) from the current precision electroweak data, and (b) from including the expected Tevatron Run-2 measurement of m_W and m_t (assuming the current central values of m_W and m_t with an error of 20 MeV and 2 GeV, respectively). Here, we have set $m_H^{\text{ref}} = 100 \text{ GeV}$ and $\Delta U = 0$ in the fit.

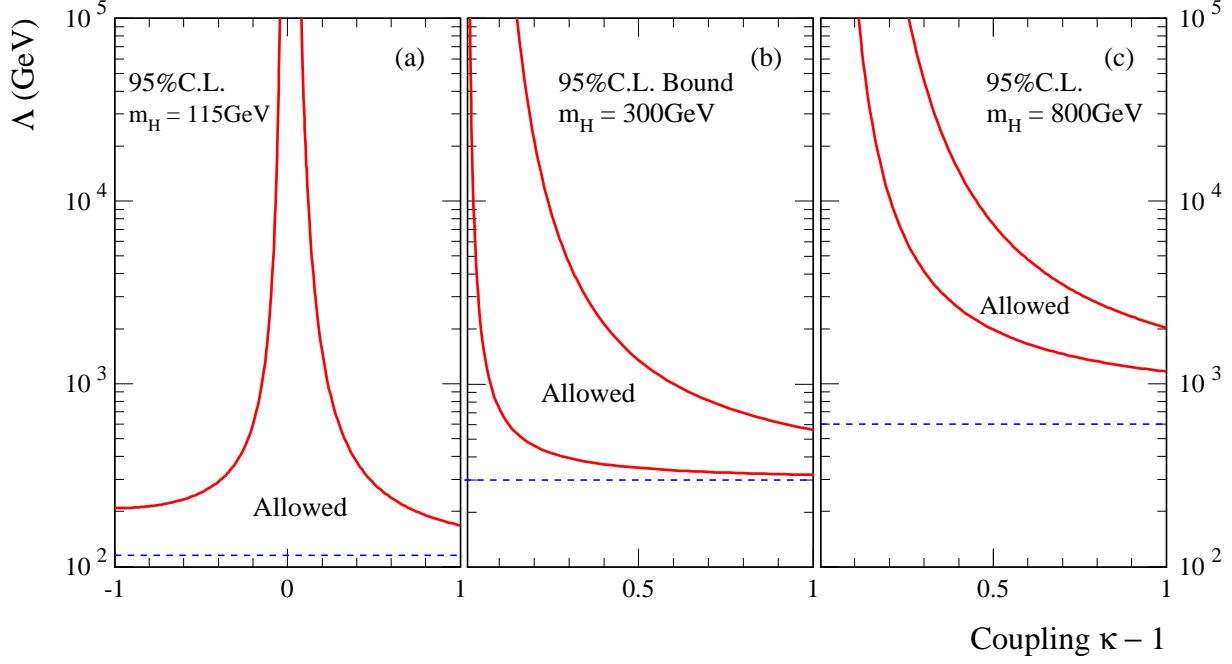


FIG. 3. Constraints on the new physics scale Λ as a function of the anomalous coupling $\Delta\kappa \equiv \kappa - 1$. The regions below the solid curves and above the dashed lines [(a)] or between the two solid curves [(b)-(c)] are allowed at the 95% C.L. The dashed lines indicate the value of $m_H^{\text{ref}} = m_H$.

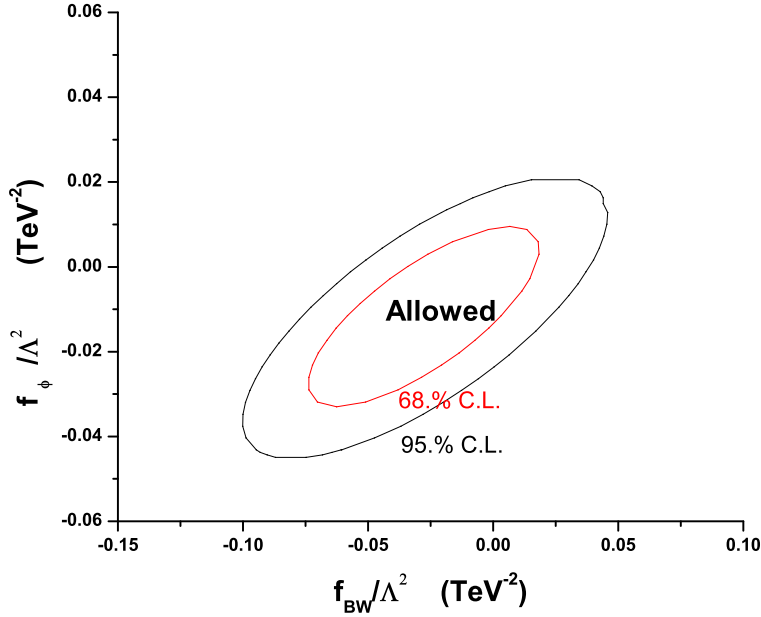


FIG. 4. The 68% and 95% C.L. bounds on f_{BW}/Λ^2 and $f_{\Phi,1}/\Lambda^2$ (in units of TeV^{-2}) from the tree level formulas of ΔS and ΔT [40] and the ΔS - ΔT bounds given in Fig. 2(a).

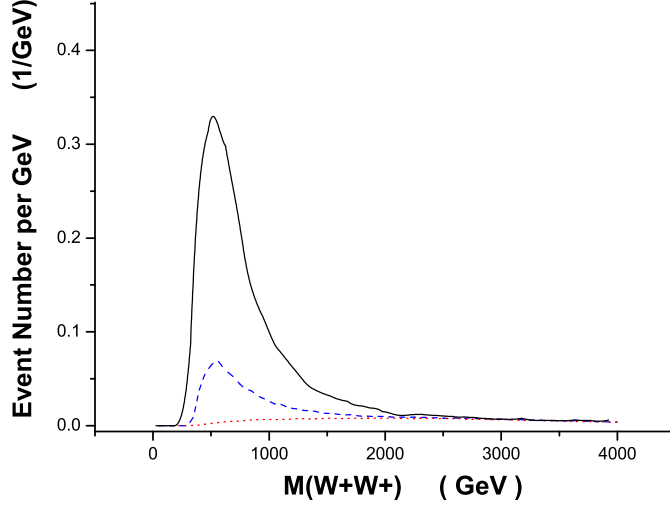


FIG. 5. Invariant mass distributions of the W^+W^+ pairs produced at the LHC for $m_H = 115$ GeV with $f_W/\Lambda^2 = f_B/\Lambda^2 = 5 \text{ TeV}^{-2}$. The solid curve is the result from the complete tree level calculation; the dashed curve is the result from the EWA calculation with the exact $W_L^+W_L^+ \rightarrow W_L^+W_L^+$ amplitude; the dotted curve is the result from the EWA calculation with the asymptotic formula [49] for the $W_L^+W_L^+ \rightarrow W_L^+W_L^+$ scattering amplitude.

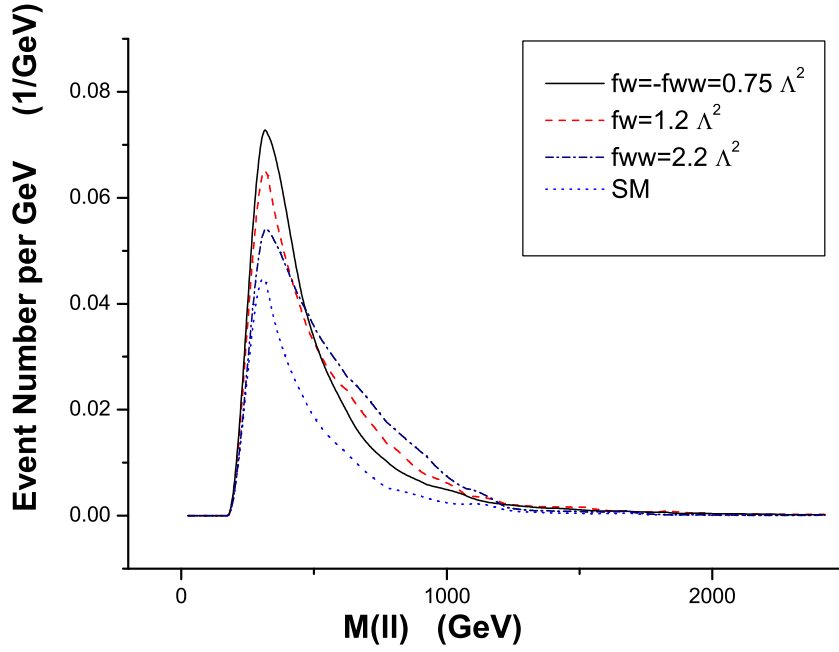


FIG. 6. Invariant mass distribution of the di-leptons from the decay of W^+ bosons produced at the LHC via $pp \rightarrow W^+W^+jj$ for $m_H = 115$ GeV with $f_W/\Lambda^2 = -f_{WW}/\Lambda^2 = 0.75 \text{ TeV}^{-2}$ [Eq. (31)] (solid line), $f_W/\Lambda^2 = 1.2 \text{ TeV}^{-2}$, $f_{WW}/\Lambda^2 = 0$ [Eq. (29)] (dashed line), $f_{WW}/\Lambda^2 = 2.2 \text{ TeV}^{-2}$, $f_W/\Lambda^2 = 0$ [Eq. (30)] (dashed-dotted line), and the SM (dotted line).